https://doi.org/10.5194/wes-2025-220
Preprint. Discussion started: 14 November 2025

eawe european academy of wind energy
Open Access WIND ENERGY SCIENCE DISCUSSIONS

A framework for the superposition of wind turbines wake properties

Ali Khanjari[1] and Cristina L. Archer[1,2]

[1]Center for Research in Wind (CReW), University of Delaware, 221 Academy St, Newark, DE 19716, USA
[2]Department of Environmental, Land, and Infrastructure Engineering (DIATI), Politecnico di Torino, Turin, Italy

Correspondence: Cristina L. Archer (carcher@udel.edu)

Abstract. Wind turbines extract kinetic energy from the wind flow and convert it to electric power, while leaving downstream complex, non-stationary, and meandering plumes of reduced wind speed and increased turbulence, called wakes. Several analytical models have been proposed in the literature to describe the structure of wake properties, such as wind speed deficit (ΔU), turbulence intensity (TI), or turbulence kinetic energy (TKE), all of which have been expressed as a function of the upstream, or undisturbed, value of said properties. While this dependency on undisturbed values is natural and practical for a single wind turbine, it becomes less so in the presence of multiple turbines, to the point of being meaningless in large wind farms, where the distance between front- and last-row turbines may exceed tens of kilometers and therefore the very concept of undisturbed flow is moot for the majority of turbines. As such, superposition methods, which aim at obtaining the final distribution of wake properties in overlapping wakes from multiple wind turbines, struggle to provide consistent results, especially for turbulence properties. In addition, the literature is lacking coherent definitions of the superposition methods, with each study introducing its own naming convention and often slightly different formulations. Here we propose a framework to standardize wake superposition for use with any analytical model of wake properties, including ΔU, TI, or TKE (but not temperature or pressure). The framework is based on the concept of "inflow", as opposed to undisturbed, values, which are in general affected by upstream turbines and are truly undisturbed only for front-row turbines. Within this framework, we propose that the inflow property should not be a constant, but rather a function of z, taken at a fixed distance upstream of each turbine, for example one diameter. Furthermore, the superposition methods are grouped into two main categories (i.e., simple or normalized summation), with the value of an exponent m controlling the linearity or non-linearity of the summed terms. The performance of the superposition methods within the framework is assessed for three analytical wake models (one for each of the three wake properties ΔU, TI, and TKE) against LES results from independent studies under various wind farm layouts, turbine models, and atmospheric stabilities. General findings are that the value of m controls the magnitude of the resulting wake property, with higher values for smaller m, and that, for the same value of m, the simple summation methods tend to create stronger overlapping wakes than the normalized ones in terms of turbulence properties, but the opposite is found for wind speed deficit. We conclude that the selection of the superposition method depends in part on the bias of the analytical wake model itself.

1 Introduction

Annual wind power production has been growing due to the increasing size and number of both onshore and offshore wind farms (Díaz and Soares, 2020). This expansion has raised critical questions about the interaction between wind farms and the

https://doi.org/10.5194/wes-2025-220
Preprint. Discussion started: 14 November 2025

eawe european academy of wind energy
Open Access WIND ENERGY SCIENCE DISCUSSIONS

atmospheric boundary layer (ABL) and about the effects of wind farms and turbines on downwind areas and other wind farms. Wind turbines convert the kinetic energy of the inflow wind into electricity, creating wake regions downstream. In a wind farm, wakes from each wind turbine cause a velocity deficit and an increased level of turbulence, which reduce the output power and increase the fatigue and dynamic loads on downwind turbines (Burton et al., 2011). The average power losses due to the wakes accounts for 10 to 20% of the total power output in large offshore wind farms (Barthelmie et al., 2009). It can even affect the power production of neighboring wind farms (Nygaard, 2014).

Turbulence is one of the main parameters to consider in studying the interaction between wind turbines and the atmospheric boundary layer and the wake region in the wind farms (Kumer et al., 2016; Porté-Agel et al., 2020). In a wind farm, turbulence is driven by atmospheric stability and wind shear and is strongly dependent on site location, season, and synoptic conditions. In large wind farms, turbulent vertical momentum flux plays a major role in efficiency (Emeis, 2018). Moreover, under relatively low offshore turbulence, strong wakes can persist and extend tens of kilometers downstream of the wind farms (Bodini et al., 2019; Platis et al., 2018; Golbazi et al., 2022). Turbulence intensity (TI), the ratio of the standard deviation of the wind speed (σ_U) to the horizontal mean flow velocity $\bar{U}$:

$$TI = \frac{\sigma_U}{\bar{U}} \tag{1}$$

has been the only variable for turbulence characterization in wind farms because it is used in the International Electrotechnical Commission (IEC) standard (International Electrotechnical Commission, 2019). However, there is much more information in the wake region than what can be captured with TI, and higher-order statistics, as well as individual turbulence intensities along each axis, should not be neglected (Morales et al., 2012; Archer, 2025). By contrast, turbulent (or turbulence) kinetic energy (TKE), defined as half of the sum of the squares of standard deviations of the three velocity components along $x, y,$ and z, is the kinetic energy per unit mass associated with the turbulent flow:

$$TKE = \frac{1}{2}\left(\sigma_u^2 + \sigma_v^2 + \sigma_w^2\right) = \frac{1}{2}\left(\overline{u'^2} + \overline{v'^2} + \overline{w'^2}\right), \tag{2}$$

where the overbar ($\bar{\cdot}$) denotes a time average and the turbulent velocity components are the difference between the instantaneous and the mean (e.g., $u' = u - \bar{u}$). TKE quantifies the energy associated with velocity fluctuations and in particular it accounts for the vertical fluctuations in the wind field, which are not accounted for with TI. In the wake region of large wind farms, the wind speed deficit is mostly replenished by vertical turbulent momentum fluxes, as resolved vertical advection is generally minimal (Siedersleben et al., 2020). TKE is therefore more suitable than TI for studying wind turbine wake effects because vertical mixing is significant.

Large-eddy simulation (LES) has been a successful numerical approach to study wind turbine wakes (Sørensen and Myken, 1992; Madsen, 1996; Sorensen and Shen, 2002; Mikkelsen, 2003; Xie and Archer, 2015, 2017; Breton et al., 2017; Ghaisas et al., 2017). Because of the high spatial and temporal resolutions, LES models are an accurate approach to study the effect of wind turbine wakes on the surrounding environment (Wu et al., 2023). However, LES cannot be used for medium- or long-term wind farm modeling because it is computationally demanding. The Weather Research and Forecast (WRF) model (Skamarock et al., 2021), a numerical weather prediction or mesoscale model, is an appropriate tool to study the wind farm interaction

https://doi.org/10.5194/wes-2025-220
Preprint. Discussion started: 14 November 2025

eawe european academy of wind energy
Open Access WIND ENERGY SCIENCE DISCUSSIONS

with the boundary layer over medium- to long-term horizons, from several days to several years. However, since the spatial resolution of WRF is not fine enough (ranging between 1 and 100 km) to explicitly treat wind turbine wakes, a wind farm parametrization (WFP) is needed. The Fitch scheme (Fitch et al., 2012) is the WFP available by default in WRF; it treats the wind turbines in a grid cell as sinks of momentum and sources of TKE. The Fitch WFP ignores the wind farm layout within a grid cell and therefore the interaction of multiple wakes cannot be simulated properly (Pan and Archer, 2018; Archer et al., 2019, 2020; Fischereit et al., 2022). Several studies have found that the Fitch scheme adds too much TKE into the grid cells of the wind farms, which results in exaggerated mixing Pan and Archer (2018); Abkar and Porté-Agel (2015); Vanderwende et al. (2016); Eriksson et al. (2015); Archer et al. (2020); on the other hand, not adding any TKE at all leads to poor agreement with LES models of wind farms Vanderwende et al. (2016). To better capture the wind speed deficit caused by the sub-grid wakes, several alternative WFP have been added in the WRF model (Ma et al., 2022b, a), referred to as the MAV wind farm parameterizations from the authors' initials, based on analytical models, discussed in the next section.

1.1 Analytical wake models

Analytical models are a preferred choice for the purposes of optimizing the wind farm layout over flat terrain compared to numerical simulation tools due to efficient computational cost (Porté-Agel et al., 2020). Most analytical wake models predict the wind speed deficit (ΔU) in a wind farm to calculate the total power production accounting for wake losses (Archer et al., 2018). The most widely used, the Jensen model (Jensen, 1983), predicts a uniform, top-hat wind speed deficit across the rotor area that expands with a constant rate as a function of distance x downstream. Since then, a series of wind speed deficit models were developed (Katic et al., 1986; Larsen, 1988; Frandsen et al., 2006; Barthelmie et al., 2004). Bastankhah and Porté-Agel (2014) proposed the first Gaussian model of the (normalized) wind speed deficit, which was later improved by Xie and Archer (2015), "XA2015" hereafter, by introducing two different expansion rates along y and z (k_y and k_z), as follows:

$$\delta U = \frac{\Delta U}{U_\infty} = \delta U(x,y,z) = \frac{U_\infty(z) - U(x,y,z)}{U_\infty(z)} = \delta_{\text{hub}} \exp\left\{ -\left[\frac{(z-H)^2}{2\sigma_z^2} + \frac{y^2}{2\sigma_y^2} \right] \right\}, \tag{3}$$

where

$$\delta_{\text{hub}} = \delta_{\text{hub}}(x) = 1 - \sqrt{1 - \frac{C_T}{8\frac{\sigma_y \sigma_z}{D^2}}}, \tag{4}$$

and

$$\frac{\sigma_y}{D} = \frac{\sigma_y(x)}{D} = k_y \frac{x}{D} + \varepsilon, \qquad \frac{\sigma_z}{D} = \frac{\sigma_z(x)}{D} = k_z \frac{x}{D} + \varepsilon, \tag{5}$$

where H and D are the turbine hub height and diameter; $C_T = C_T(U_H)$ is the thrust coefficient, typically provided by the turbine manufacturer as a function of hub height wind speed (U_H); $U_\infty(z)$ is the undisturbed vertical wind speed profile; ε is a function of C_T (see Eq. 37 in XA2015). The XA2015 analytical model will be used later as the benchmark for wind speed deficit.

https://doi.org/10.5194/wes-2025-220
Preprint. Discussion started: 14 November 2025

eawe european academy of wind energy
Open Access WIND ENERGY SCIENCE DISCUSSIONS

As for added turbulence, most analytical models in the literature have used turbulence intensity (TI) as the relevant variable. Quarton and Ainslie (1990) suggested the first empirical formulation that relates the maximum added TI behind a wind turbine (ΔTI) to the freestream turbulence intensity (TI_∞) and the thrust coefficient. Crespo and Hernández (1996) proposed an analytical function that provides the maximum ΔTI separately for the near wake ($x < 3D$, where the effects of the rotor geometry are dominant, with steep gradients of pressure and axial velocity, and wake expansion) and the far wake ($x \geq 3D$, where the effect of rotor geometry is insignificant on the wind flow, and the wake is mainly influenced by the atmospheric turbulence generated by wind shear associated to the wind speed deficit and by entrainment processes).

Ishihara and Qian (2018) provided the first three-dimensional analytical equation for TI added by a wind turbine as a Gaussian function in the radial direction r (from the center of the rotor) multiplied by an amplitude function (an inverse function of x), as follows:

$$\Delta TI(x,y,z) = \frac{1}{d + e\frac{x}{D} + f\left(1+\frac{x}{D}\right)^{-2}} \times \left\{ k_1 \exp\left[-\frac{\left(r-\frac{D}{2}\right)^2}{2\sigma^2} \right] + k_2 \exp\left[-\frac{\left(r+\frac{D}{2}\right)^2}{2\sigma^2} \right] \right\} - \delta(z) \tag{6}$$

$$\delta(z) = \begin{cases} 0 & z \geq H \\ TI_\infty \sin\left(\pi \dfrac{H-z}{H}\right)^2 & z < H, \end{cases} \tag{7}$$

where d, e, f, k_1, k_2, and σ are functions of C_T and TI_∞ of the form $aC_T^b TI_\infty^c$ and the $\delta(z)$ term was later slightly modified as follows by Qian and Ishihara (2021), hereafter "QI2021":

$$\delta(z) = \begin{cases} 0 & z \geq H \\ TI_\infty \sin^2\left(\pi \dfrac{H-z}{H}\right) \cos^2\left(\pi \dfrac{y}{D}\right) & 0 \leq z < H, |y| \leq D \end{cases} \tag{8}$$

Note that the $\delta(z)$ term, whether obtained with Eq. 7 or 8, is always positive for $z < H$ and is not a function of x; therefore, given the minus sign in front of it, it will always subtract a fixed amount of TI from the region below the rotor for all streamwise distances, which is unrealistic. The QI2021 model will be used as the benchmark for added TI in this study.

Later, Tian et al. (2022) developed a three-dimensional cosine-shape model to estimate the wake ΔTI by redistributing it along the radial direction with a dual-cosine shape function. Similarly, Li et al. (2022) proposed a three-dimensional analytical formula for added turbulence intensity. They also found that the added turbulence intensity, ΔTI, in the streamwise direction exhibits a self-similarity property similar to that of the velocity deficit.

Only two studies have used TKE, rather than TI, as the variable of choice to study turbulence in wind turbine wakes. The most recent study based on TKE was that by Bastankhah et al. (2024) who, by analytically solving the TKE transport partial differential equation using the Green's function method, developed a model predicting the three-dimensional distribution of added TKE (ΔTKE) of a single turbine as a function of r and x:

https://doi.org/10.5194/wes-2025-220
Preprint. Discussion started: 14 November 2025

eawe european academy of wind energy
Open Access WIND ENERGY SCIENCE DISCUSSIONS

$$\Delta TKE(x,r) = \int_{X=x_0}^{x} \int_{\rho=0}^{\infty} \frac{\nu_t(X)}{2U_0\phi(X,x)} \times \exp\left\{\frac{-r^2+\rho^2}{4\phi(X,x)} - \psi(X,x)\right\} \times I_0\left(\frac{r\rho}{2\phi(X,x)}\right)\left(\frac{\partial U(X,\rho)}{\partial \rho}\right)^2 \rho\, d\rho\, dX \tag{9}$$

where I_0 is the modified Bessel function of the first kind; U is the wake velocity profile; ψ and ϕ are two positive, monotonic functions; ν_t is the turbulent viscosity; and ρ is a dummy variable. Since this model requires the integration of the wind speed deficit squared, multiplied by tree other functions, which is only obtainable in a few simplified cases, it will not be used in the rest of this study.

In an earlier study, Khanjari et al. (2025) developed a three-dimensional analytical model for ΔTKE in the wake region of a single turbine as a function of undisturbed hub-height turbulence intensity $TI_\infty(H)$, undisturbed hub-height wind speed $U_\infty(H)$, D, H, and C_T. They showed that their proposed model is in good agreement with LES and wind tunnel data under different atmospheric stabilities and turbine characteristics. Their analytical model was therefore selected as the benchmark for added TKE in this study (called "KA2025" hereafter) and will be described in more detail in Section 2.1.

1.2 Superposition methods

The wake models described so far are valid for the wake region of a single turbine. In a wind farm, wakes from several wind turbines may overlap and the resulting wind speed deficit or added turbulence need to be calculated via so-called superposition methods. Again, the literature about superposition methods for the wind speed deficit is richer than that for added turbulence and it will be briefly reviewed next; more details can be found in Porté-Agel et al. (2020). The two most common superposition methods to obtain the wind speed U at location x, y, z downstream of N wind turbines are the linear one (Lissaman, 1979):

$$U = U_\infty - \sum_{i=1}^{N} \Delta U_i, \tag{10}$$

and the squared one (Katic et al., 1986):

$$U = U_\infty - \sqrt{\sum_{i=1}^{N} (\Delta U_i)^2}, \tag{11}$$

where:

$$\Delta U_i = \Delta U_i(x,y,z) = U_\infty - U_i \tag{12}$$

is the wind speed deficit caused by turbine i alone, estimated for example via Eq. 3, and $U_i = U_i(x,y,z)$ is the wind speed downstream of turbine i. Note that U_∞ is assumed to be the same for all the turbines.

As the incoming wind speed of each turbine i is not necessarily equal to U_∞, Voutsinas et al. (1990) proposed an alternative method to correct the ΔU_i in Eq. 12 as follows:

$$\Delta U_i = U_{in,i} - U_i, \tag{13}$$

https://doi.org/10.5194/wes-2025-220
Preprint. Discussion started: 14 November 2025

eawe european academy of wind energy
Open Access WIND ENERGY SCIENCE DISCUSSIONS

where $U_{in,i}$ is the "inflow" velocity experienced by turbine i (coinciding with the true undisturbed upstream wind speed U_∞ only for the front-row turbines) as a result of all the turbines upstream of it:

$$U_{in,i} = U(x_i, y_i) \tag{14}$$

where x_i, y_i are the coordinates of turbine i and U is given by either Eq. 10 or 11. Because the hub itself introduces disturbances in the wind flow right upstream of the turbine location, the inflow wind speed is sometimes taken at a distance of $-2.5D$ to $-1D$ upstream of the turbine, sufficient to avoid such disturbances.

The exact definition of both undisturbed and inflow wind speed depends on the application. If the goal is to estimate just hub-height wind speed, then the $U_{in,i}$ and U_∞ values are to be considered at hub height, thus $U_{in,i} = U(x_i, y_i, H)$ and $U_\infty = U_\infty(H)$; if the goal is to estimate the full spatial distribution of wind speed (e.g., if wind shear is important), then $U_{in,i} = U_{in,i}(z)$ and $U_\infty = U_\infty(z)$. Note that $U_i = U_i(x, y, z)$ and $\Delta U_i = \Delta U_i(x, y, z)$ regardless of the dimensions of $U_{in,i}$.

Several studies have focused on turbulence superposition models, most of which used TI as the relevant variable. Similar to wind speed deficit, the goal of the TI superposition method is to obtain an expression for the turbulence intensity at location x, y, z downstream of N turbines, each of which alone would add ΔTI_i. Qian and Ishihara (2021) developed the first TI superposition model based on the linear sum of squares (LSS) of turbulence variances, inspired by the IEC 61400-1 standard (International Electrotechnical Commission, 2019, Eq. E.3):

$$TI = \sqrt{{TI_\infty}^2 + \sum_{i=1}^{N} (\Delta TI_i + \alpha_{ij})^2}, \tag{15}$$

where α_{ij} is an empirical correction term that depends only on the turbine j that is the nearest upstream from i and that should only be used with the analytical model for added TI by Ishihara and Qian (2018), shown in Eq. 6. They investigated it for both an in-line and a partially-offset layout and found that Eq. 15 delivers accurate predictions for an offshore wind farm based on LES runs.

Like with Eq. E.3 of the IEC 61400-1 standard, the issue with the LSS method in Eq. 15 is that it does not reconstruct the TI added by the first turbine correctly. For the first turbine, $\alpha_{ij} = 0$ and the TI downstream of it should be just $TI_\infty + \Delta TI_1$; with Eq. 15, however, the resulting TI is instead $\sqrt{TI_\infty^2 + (\Delta TI_1)^2} \neq TI_\infty + \Delta TI_1$. Because of this nonphysical behavior, the LSS method is not recommended for wake turbulence superposition.

Like for undisturbed wind speed, only the front-row turbines (i.e., the most upstream) experience the truly undisturbed TI_∞, while the others experience $TI_{in,i}$, the "inflow" TI, generally different from TI_∞ because $TI_{in,i}$ is the result of all the turbines upstream of i combined. Note that the inflow TI of the first (or front-row) turbine(s) is $TI_{in,1} = TI_\infty$. This concept was implicitly introduced by Zhang et al. (2022), who compared the performance of four different TI superposition models, discussed next, for four in-line turbines from LES runs under different values of U_∞ and TI_∞. The first two are the geometric superposition method:

$$TI = TI_\infty \prod_{i=1}^{N} \frac{TI_i}{TI_{in,i}}, \tag{16}$$

https://doi.org/10.5194/wes-2025-220
Preprint. Discussion started: 14 November 2025

eawe european academy of wind energy
Open Access WIND ENERGY SCIENCE DISCUSSIONS

and the kinetic energy deficit method:

$$TI = \sqrt{{TI_\infty}^2 + \sum_{i=1}^{N} \left(TI_i^2 - TI_{in,i}^2\right)}, \tag{17}$$

where TI_i is the TI downstream of turbine i alone and $TI_{in,i} = TI(x_i, y_i, z)$ is the inflow TI at turbine i located at x_i, y_i. Like in Eq. 14, since the hub itself can cause localized turbulence, a location $-1D$ upstream of the turbine can be used for $TI_{in,i} = TI(x_i - 1D, y_i, z)$. Because the geometric and kinetic energy deficit methods do not isolate the TI added by each wind turbine, they cannot easily be implemented in a WFP and therefore will not be considered further in this study.

The other two methods proposed by Zhang et al. (2022) are the (normalized) linear method:

$$TI = TI_\infty \left[1 + \sum_{i=1}^{N} \frac{\Delta TI_i}{TI_{in,i}}\right], \tag{18}$$

and the (normalized) squared summation method:

$$TI = TI_\infty \left\{1 + \left[\sum_{i=1}^{N} \left(\frac{\Delta TI_i}{TI_{in,i}}\right)^2\right]^{1/2}\right\} \tag{19}$$

where ΔTI_i is the added TI downstream of turbine i alone ($\Delta TI_i = TI_i - TI_{in,i}$). Note that these two methods are denoted as normalized (in parenthesis) because they are based on added TI normalized by $TI_{in,i}$. In addition, Zhang et al. (2022) proposed an exponential (normalized) superposition method:

$$TI = TI_\infty \left\{1 + \left[\sum_{i=1}^{N} \left(\frac{\Delta TI_i}{TI_{in,i}}\right)^m\right]^{1/m}\right\} \tag{20}$$

where $m = 0.8$. The notation used here for Eqs. 16–20 is slightly different from that originally introduced by Zhang et al. (2022), but it retains the full meaning of their formulations while being consistent with the notation used earlier for the wind speed deficit ΔU. The focus of the original formulation by Zhang et al. (2022) was on TI at the locations of the turbines (thus their index i was for the turbine of interest and j for the upstream turbines), while our focus is on any location x, y, z downstream of the turbines (thus TI has no subscript on the left-hand side of Eqs. 16–20 and i is the index for the upstream turbines).

The literature is rather unclear about how to properly define and calculate the terms $TI_{in,i}$, including $TI_\infty = TI_{in,1}$. Like the $U_{in,i}$ terms in the wind speed deficits, the TI_∞ and $TI_{in,i}$ terms too can be taken at hub height [$TI_\infty(H)$ and $TI_{in,i}(H)$] or their dependency on z can be retained [$TI_\infty(z)$ and $TI_{in,i}(z)$]. The original notation in Zhang et al. (2022) does not specify how to calculate them, but, in a personal communication, the authors explained that the $TI_{in,i}$ terms are to be calculated by taking a spatial average of the TI over the area of the rotor disk at a specific upstream location (e.g., $-1D$). They reported that Eq. 20 agrees better with the LES model of in-line turbines at Lillgrund and Horns Rev wind farms compared to the other four superposition models if this convention is adopted. However, as discussed later and demonstrated in the Appendix in Fig. A1b, using a constant value for $TI_{in,i}$, whether at hub height or a rotor-average, introduces inconsistencies in the superposition and is therefore not recommended.

https://doi.org/10.5194/wes-2025-220
Preprint. Discussion started: 14 November 2025

eawe european academy of wind energy
Open Access WIND ENERGY SCIENCE DISCUSSIONS

Since the turbine-added turbulence is very small or even negative below the hub height due to ground effects and reduced shear (Archer et al., 2019; Wu et al., 2023), superposition methods often produce weak predictions in this region. Li et al. (2023) proposed a normalized superposition model of TI that comprises two parts, to handle both negative and positive values of added TI:

$$\Delta TI = \begin{cases} \left[\sum_{i=1}^{n} (\Delta TI_i)^{2.5}\right]^{\frac{1}{2.5}}, & \Delta TI_i(x,y,z) > 0 \\ \max\{\Delta TI_i\}, & \Delta TI_i(x,y,z) < 0 \end{cases} \tag{21}$$

Then, similar to Zhang et al. (2022), they compared the results of their proposed model with the linear summation method:

$$\Delta TI = \sum_{i=1}^{N} (\Delta TI_i) \tag{22}$$

and the squared summation method:

$$\Delta TI = \sqrt{\sum_{i=1}^{N} (\Delta TI_i)^2}. \tag{23}$$

They considered two definitions for ΔTI_i: $\Delta TI_i = TI_i - TI_{in,i}$, called "rotor-based" added turbulence intensity, and $\Delta TI_i = TI_i - TI_\infty$, called "ambient-based" added turbulence intensity; a similar classification was also introduced for the undisturbed wind speed by Porté-Agel et al. (2020). Physically, the ambient-based definition is the correct choice for front-row turbine(s) and the rotor-based definition for the rest.

A few combinations and minor variations of the above superposition methods for added TI have later been proposed and evaluated against numerical results based on the Reynolds-averaged Navier-Stokes (RANS) equations by Risco et al. (2023) and Delvaux et al. (2024), which reached contradictory conclusions: the latter indicated that the kinetic energy deficit method (Eq. 17, called simply "Square" in their paper) performed best, while the former showed that the linear method (Eq. 22) provided the best agreement with the RANS results. Delvaux et al. (2024) pointed out that the very definition of ΔTI may be an additional complicating factor when it is derived from TKE, which is often the case with LES or RANS results.

In this paper, we will combine and standardize the approaches used in the literature to account for the superposition of wake properties (i.e., TKE, TI, and wind speed) in a coherent framework. However, more attention will be devoted to TKE because properly calculating TKE superposition represents a missing step towards ultimately developing a WFP that accounts for turbulence, not just wind speed deficit, induced by sub-grid wakes in mesoscale models and because TI is not a variable predicted in any mesoscale model. The ΔTKE model proposed by KA2025 (Section 2.1), the ΔTI model by QI2021 (Eq. 6), and the δU model by XA2015 (Eq. 3) will be tested in the proposed framework for wake properties superposition (Section 2.2) and evaluated with a suite of three independent LES datasets (Section 3). Insights and recommendations will be part of the last Section 4.

https://doi.org/10.5194/wes-2025-220
Preprint. Discussion started: 14 November 2025

2 Methods

2.1 The added TKE model

For added TKE, we use the analytical equation proposed by KA2025, normalized by the square of the upstream hub-height wind speed $U_\infty = U_\infty(H)$. This equation is the product of three functions: a streamwise function $A(x)$, a radial function $G(r)$, and a vertical function $W(z)$:

$$\frac{\Delta TKE}{U_\infty^2} = \delta TKE(x,y,z) = \alpha \times A(x) \times G(r) \times W(z). \tag{24}$$

The tuning parameter α is utilized to control the amplitude of $\Delta TKE/U_\infty^2$ in the wake. The streamwise function $A(x)$ follows a Weibull-like shape:

$$A(x) = \left(\frac{x - x_0}{\lambda_A}\right)^{k_A - 1} exp\left[-\left(\frac{x - x_0}{\lambda_A}\right)^{k_A}\right], \tag{25}$$

where λ_A and k_A are the scale and shape parameters of the Weibull distribution. The radial $G(r)$ follows a Gaussian shape along the radial direction which peaks at the annular edges of the rotor as follows:

$$G(r) = \exp\left[-\frac{(r - D/2)^2}{2\sigma_r^2}\right], \tag{26}$$

where $r = \sqrt{(y - y_0)^2 + (z - H)^2}$, y_0 is the spanwise location of the turbine, and σ_r is a linear function of x:

$$\sigma_r(x) = k_r\,(x - x_0) + \varepsilon_r D, \tag{27}$$

where k_r is the radial expansion rate (i.e., $\frac{\partial \sigma_r}{\partial x}$) and ε_r is a multiplying factor to the rotor diameter that sets the initial width of the Gaussian distribution of the added TKE along the annulus of the rotor disk. Lastly, the vertical function $W(z)$ is also assumed to be Weibull-like:

$$W(z) = \left(\frac{z}{\lambda_W}\right)^{k_W - 1} exp\left[-\left(\frac{z}{\lambda_W}\right)^{k_W}\right], \tag{28}$$

where the shape parameter k_W is set equal to 4.

In summary, the equation for $\Delta TKE/U_\infty^2$ (Eq. 24) contains five unknown parameters: $\alpha, \lambda_A, \lambda_W, k_r$, and ε_r. Khanjari et al. (2025) proposed that α, k_r, and ε_r depend on C_T and $TI_\infty = TI_\infty(H)$ with the following general form:

$$a\, C_T^b\, TI_\infty^c, \tag{29}$$

whereas λ_A and λ_W include an additional dependency on D and H as follows:

$$\lambda_A = a\, D\, C_T^b\, TI_\infty^c, \tag{30}$$

https://doi.org/10.5194/wes-2025-220
Preprint. Discussion started: 14 November 2025

eawe european academy of wind energy
Open Access WIND ENERGY SCIENCE DISCUSSIONS

$$\lambda_W = H + a\ D\ C_T^b\ TI_\infty^c. \tag{31}$$

The parameters a, b, and c were obtained by KA2025 by curve-fitting against several LES datasets of added TKE behind single turbines under different stability conditions and their values are reported in Table 1.

Table 1. Functional relationships for the five fitting parameters from Khanjari et al. (2025).

	α	λ_A	λ_W	k_r	ε_r
	(-)	(m)	(m)	(-)	(-)
Equation	$a\ C_T^b\ TI_\infty^c$	$a\ D\ C_T^b\ TI_\infty^c$	$H + a\ D\ C_T^b\ TI_\infty^c$	$a\ C_T^b\ TI_\infty^c$	$a\ C_T^b\ TI_\infty^c$
a	0.217	3.938	1.384	0.480	0.411
b	2.269	-0.472	-0.429	0	0.728
c	0	-0.281	0.541	1.105	0.298

2.2 The proposed framework for wake properties superposition

The first step of the proposed wake superposition framework is a proper, physically informed, definition of the background or undisturbed values (i.e., those with the ∞ subscript). This concept is not straightforward. For a single turbine, it is the value of the property of interest $\mathcal{P}$ (where $\mathcal{P}$ can be wind speed or TI or TKE) upstream of the turbine that has not been affected by the turbine itself. How far upstream one needs to go to obtain a truly undisturbed value is, however, complicated because induction effects, although small in magnitude, have been measured as far upstream as $-4D$ (Medici et al., 2011; Simley et al., 2016; Porté-Agel et al., 2020). In addition, in a wind farm, only the front-row wind turbines experience the undisturbed flow, while the rest of them are in fact "disturbed" by the very presence of upstream wind turbines. The latter issue has been captured in the literature by the concept of "inflow" property $\mathcal{P}_{in}$, which is the equivalent of $\mathcal{P}_\infty$ but for the turbines that are not front-row. With this in mind, we introduce the following four propositions.

The first is that the undisturbed property $\mathcal{P}_\infty$ is actually a special case of the inflow property $\mathcal{P}_{in}$, not vice versa, which we can write as follows:

$$\mathcal{P}_\infty = \mathcal{P}_{in,1} \tag{32}$$

where the index 1 indicates the front-row turbine(s). Any added property by a turbine i should therefore be calculated by default based on the inflow value:

$$\Delta\mathcal{P}_i = \mathcal{P}_i - \mathcal{P}_{in,i} \tag{33}$$

https://doi.org/10.5194/wes-2025-220
Preprint. Discussion started: 14 November 2025

eawe european academy of wind energy
Open Access WIND ENERGY SCIENCE DISCUSSIONS

(except $\Delta U = U_{in,i} - U_i$) and the inflow value should also be the one used at the denominator to normalize the property, if needed. This proposition is aligned with the literature, as similar considerations were introduced for example by Porté-Agel et al. (2020), who differentiated the "boundary-layer flow speed" from the "incoming flow speed", or by Li et al. (2022), who introduced a "rotor-added" and an "ambient-based" added TI. Furthermore, this assumption is necessary in mesoscale model applications where the wind farm is partitioned over multiple grid cells. In such cases, it may be difficult to identify which grid cell should be treated as undisturbed, especially in the presence of intra-farm changes in wind direction. The value of $\mathcal{P}$ in each grid cell, by contrast, is a straightforward choice for $\mathcal{P}_{in}$.

The second proposition is that there should be a default location upstream of each turbine i at which to obtain the values of $\mathcal{P}_{in,i}$, including $\mathcal{P}_{\infty,i}$, and this location should be clearly specified. Here we propose the point located $-1D$ upstream of each turbine (Simley et al., 2016), including the front-row, thus:

$$\mathcal{P}_{in,i} = \mathcal{P}(x_i - 1D, y_i), \tag{34}$$

where x_i, y_i are the coordinates of turbine i. The sensitivity to the default location selection, including possibly the effect of the induction (Vollmer et al., 2024), should be the focus of future investigations.

Shifting the focus from the upstream to the downstream region, wind turbine wakes eventually dissipate and the property of interest recovers to its undisturbed profile. While the IEC standard uses $10D$ as the maximum distance after which turbulence effects are supposed to vanish, evidence from the literature (e.g., Fig. 15 in Wu et al., 2023) indicates that TKE added by wind turbines can last even past $20D$. Physically, it would be preferred not to impose such a threshold because the analytical TKE model should decay enough to asymptotically reach recovery; however, if a threshold must be imposed, e.g., to expedite numerical calculations, then $20D$ is the recommended value for the maximum streamwise extent. For the lateral expansion, a maximum width of $3D - 4D$ is sufficient (Wu et al., 2023, Fig. 15).

The third proposition is that the inflow property should be a function of z by default, not a constant (from the literature, it is typically its value at hub height):

$$\mathcal{P}_{in} = \mathcal{P}_{in}(z), \tag{35}$$

otherwise the superposition methods may introduce nonphysical features in the three-dimensional structure of the wake property. To understand why, let us consider a normalized added TI formulation with a constant value for $TI_{in}(H)$ at the denominator in Eq. 18 and focus on a level z_2 near the ground, where turbulence is generally high and therefore $TI_\infty(z_2) > TI_\infty(H)$ at any x, y. The distribution of TI downstream of the first wind turbine ($i = 1$) from Eq. 18 is $TI(z_2) = TI_\infty(z_2) + TI_\infty(z_2)\frac{\Delta TI_1(z_2)}{TI_\infty(H)}$, which is incorrect and larger than the real $TI(z_2) = TI_\infty(z_2) + \Delta TI_1(z_2)$. This issue does not affect just the first turbine(s), but all of them. As can be appreciated in Fig. A1b, the superposition with a constant value $TI_{in}(H)$ used to normalize the added TI causes an underestimate for $z > H$ and a slight overestimate for $z < H$. The only vertical level for which a constant value of $TI_{in}(H)$ would lead to the correct value of TI is $z = H$; for all other levels it would lead to inaccurate results. Thus, the use of a constant value $TI_\infty(H)$ is perfectly adequate only for those special cases where the three-dimensionality of the wake is not important because only the values at hub height are desired, e.g. in wake loss models for wind power generation. The same issue is also found for TKE in Fig. A1a.

https://doi.org/10.5194/wes-2025-220
Preprint. Discussion started: 14 November 2025

eawe european academy of wind energy
Open Access WIND ENERGY SCIENCE DISCUSSIONS

Lastly, from the literature, the methods to calculate a wake property superposition can be grouped into two main approaches: the first, named "simple summation", is based on the summation of the added property to the background, and the second, called "normalized summation", is based on the summation of the normalized added property. Both types can be utilized in conjunction with any value of the exponent m used to raise the $\Delta\mathcal{P}$ term. Here we will focus on three values of m (0.8, 1, or 2) because they are the only three that have been used in the literature. The formulation with $m = 1$ is a linear sum, that with $m = 2$ is a linear sum of squares, and that with $m = 0.8$ is known as exponential (Zhang et al., 2022). Even though none of them is derived from physical principles, there is no evidence in the past literature that one approach might outperform the other.

Hereafter we assume that a total of N_{tot} wind turbines have been arranged in such a way that the first one is the most upstream, or front-row ($i = 1$), the second is the second most upstream ($i = 2$), etc. There can be multiple wind turbines in the same front-row position and, for any location x, y, z, there are $N \leq N_{tot}$ upstream wind turbines in total. Thus N is technically a function of i, but, for consistency with the literature, we are omitting the subscript i. With these conventions, we can define the normalized summation (NS) method as:

$$\mathcal{P} = \mathcal{P}(x,y,z) = \mathcal{P}_\infty(z) \left\{ 1 + \left[\sum_{i=1}^{N} \left(\frac{\Delta\mathcal{P}_i}{\mathcal{P}_{in,i}(z)} \right)^m \right]^{1/m} \right\} \tag{36}$$

and the simple summation (SS) method as:

$$\mathcal{P} = \mathcal{P}(x,y,z) = \mathcal{P}_\infty(z) + \left[\sum_{j=1}^{N} (\Delta\mathcal{P}_i)^m \right]^{1/m}, \tag{37}$$

where N is the number of wind turbines upstream of the location of interest x, y, z, $\mathcal{P}_\infty(z)$ is the undisturbed $\mathcal{P}$, $\mathcal{P}_{in,i}(z)$ is the inflow $\mathcal{P}$ profile at $-1D$ from the location of turbine i $(x_i - 1D, y_i)$, and $\Delta\mathcal{P}_i$ is the added property at a location downstream of turbine i as if it was alone and is provided by an analytical model. If $\mathcal{P} = U$, the $+$ sign in Eqs. 36–37 should be replaced with a $-$ sign; in addition, the normalized wind speed deficit δU (as in Eq. 3), should be used for the ratio $\frac{\Delta\mathcal{P}_i}{\mathcal{P}_{in,i}}$.

The analytical models for: added TKE by KA2025 from Eq. 24, added TI by QI2020 from Eq. 6, and wind speed deficit by XA2015 from Eq. 12 will be used in the rest of this paper to study the differences between the wake superpositions methods, thus in Eqs. 36 – 37 the property $\mathcal{P}$ is equal to TKE, TI, and U, respectively. However, as mentioned in the Introduction, the main focus will be on TKE.

Note that, for added TKE and added TI, $U_{in,i}(H)$ is also needed to calculate the value of C_T in Eqs. 29–31 and Eq. 6. We obtain it with the XA2015 model with the M3 superposition method of wind speed deficit from Eqs. 11 and 13, which coincides with the SS method in Eq. 37 with $m = 2$. Other combinations of the XA2015 wind speed deficit with the various superposition methods will be also assessed in Section 3, but this combination was the best performing one, in line with the literature (Archer et al., 2018; Ma et al., 2022a).

https://doi.org/10.5194/wes-2025-220
Preprint. Discussion started: 14 November 2025

eawe european academy of wind energy
Open Access WIND ENERGY SCIENCE DISCUSSIONS

The amount of added TKE by a single wind turbine depends also, from Eqs. 29–31, on $TI_\infty(H)$, which itself can be approximately obtained from $TKE_\infty(H)$, assuming isotropy, as follows:

$$TI_\infty(H) = \frac{\sqrt{\frac{2}{3}TKE_\infty(H)}}{U_\infty(H)}. \tag{38}$$

However, for use with multiple wind turbines and with the superposition methods in Eqs. 36 – 37, $TI_\infty(H)$ should be replaced with $TI_{in,i}(H)$ (except for the front-row turbines) in Eqs. 29–31.

While the steps to calculate the wind speed deficit and resulting wind speed with the XA2015 model are straightforward, as long as the wind turbines are arranged in decreasing order of distance from the front row, a precise sequence of steps needs to be followed in order to obtain the correct values of all the parameters needed to calculate TI or TKE at the location of interest in the wake of N_{tot} turbines. The workflow of these steps is presented in Fig. 1.

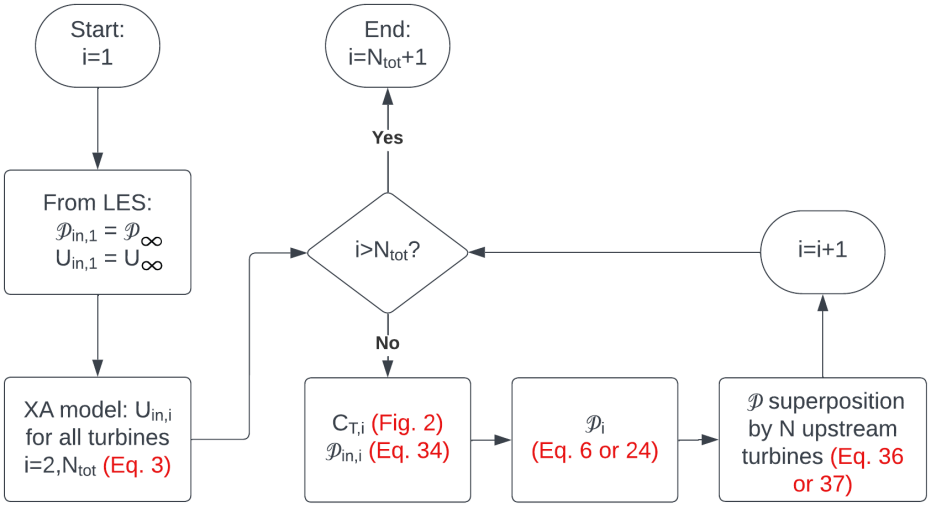

Figure 1. Flowchart of the steps required for the superposition of $\mathcal{P}$=TKE and $\mathcal{P}$=TI with the KA2025 and QI2020 analytical models, respectively. Note that the N_{tot} turbines are to be arranged in such a way that the first one ($i = 1$) is the most upstream one and the other turbines (i) follow based on their increasing distance from it; N is the number of upstream turbines at a given location downstream of turbine i, thus its value is updated at each iteration.

2.3 The LES datasets for validation

We use three previously-published LES datasets, all of which are briefly described next, to evaluate the two TKE superposition methods in Eqs. 18–20. The first, hereafter referred to as "WRFLES", was generated by Wu et al. (2023) to investigate overlapping wakes under three stability conditions (stable, neutral, and unstable) within two one-way nested domains with 15 m and 5 m horizontal resolution. The numerical code was the LES-version of the WRF model and the wind turbines were modeled

https://doi.org/10.5194/wes-2025-220
Preprint. Discussion started: 14 November 2025

eawe european academy of wind energy
Open Access WIND ENERGY SCIENCE DISCUSSIONS

with the generalized actuator disk parameterization by Mirocha et al. (2014) based on the PSU 1.5-MW Schmitz (2012) wind turbine (Figure 2). The layout consisted of three in-line turbines with D = 77 m and H = 80 m with a streamwise spacing of 7.3 m. The atmospheric stability was controlled by the surface heat flux.

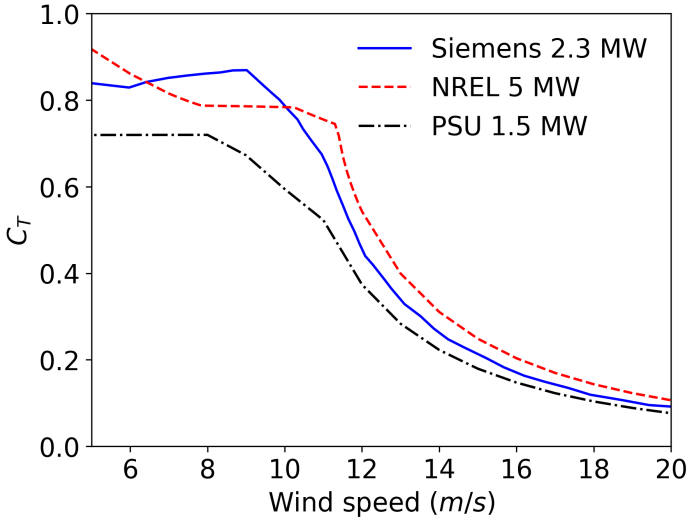

Figure 2. Thrust coefficient of the three wind turbines used in this study as a function of hub-height wind speed.

The second LES dataset is called "JHU" dataset from Johns Hopkins University (Johns Hopkins University, 2025; Zhu et al., 2025) contains LES results of a neutrally-stratified atmospheric boundary layer over a large wind farm, conducted using the concurrent-precursor inflow method. The size of the computational domain is 28,224 m × 3,780 m × 2,000 m and it is discretized to 3,072 × 384 × 400 grid-points with grid resolutions of 9.2 m along the streamwise (x) axis, 9.8 m across the transverse (y) axis, and 5 m in the vertical (z) direction. The wind farm consists of 60 NREL-5MW turbines with D=126 m and H=90 m (Fig. 2) arranged in 6 columns and 10 rows. The flow is driven by a geostrophic wind speed of 15 m/s and the Coriolis frequency is $1 \times 10^{-4} s^{-1}$. Only the southern-most column of 10 in-line wind turbines was utilized in this study.

Lastly, the "SOWFA" dataset is named from the acronym of the Software for On/Offshore Wind Farm Applications (Churchfield et al., 2012; Archer et al., 2013) that was used. It consists of a subset of the results by Ghaisas et al. (2017), who employed the SOWFA solver under stable atmospheric stability over a complex mesh of 4000 m × 4000 m × 1000 m with fine resolution (3.5 m) around 26 Siemens 2.3-MW wind turbines (D = 93 m, H = 63.4 m), parameterized as actuator lines, and coarser resolution (7 m) in the rest of the domain. The case considered here is that of westerly flow with a streamline spacing of about $10D$.

The layouts of the three LES domains are shown (not in scale) in Fig. A2.

https://doi.org/10.5194/wes-2025-220
Preprint. Discussion started: 14 November 2025

eawe european academy of wind energy
Open Access WIND ENERGY SCIENCE DISCUSSIONS

3 Results

The first property that we will consider is $\mathcal{P} = U$. Because wind speed deficit superposition has been studied extensively in the literature, here we limit our analysis to the wind speed at hub height of each turbine, as $U_{in,i}(H)$ is the input variable to obtain the C_T value from Fig. 2 and to calculate TKE from Eq. 24 for KA2025 (Fig. 1) and TI from Eq. 6 for QI2021. The benchmark model XA2015 is a normalized formulation by design because it provides an analytical equation for the normalized wind speed deficit. As such, it is expected that the NS superposition methods outperform the SS ones. However, as shown in Fig. 3, the NS methods quickly create non-realistic zero wind speeds in the wake of the inner turbines, whereas the SS methods do not present this issue.

To identify the best combination for the wind speed superposition with the XA model, we calculated the root-mean square error over the cylinder centered around the rotor and with a length of $6D$ downstream of each turbine, from $1D$ to $7D$ (Fig. 4). The best performance was achieved with the SS method with $m = 2$, which is the exact equivalent of the M3 method in Ma et al. (2022a), although the performance of the NS method with $m = 2$ was close. We then extracted the point-value of the $U_{in,i}$ at hub height at $-1D$ of each turbine and evaluated the percent error as follows:

$$\left| \frac{U_{in,i}^{XA} - U_{in,i}^{LES}}{U_{in,i}^{LES}} \right| \times 100\% \tag{39}$$

for the same layouts and flow conditions of the three LES datasets described in Section 2.3. The percent error for most turbines was rather small and less than 8% (Fig. A2), consistent with its good performance demonstrated in the past (Archer et al., 2018). The worst performance was for the second and third turbine of the WRFLES-U dataset, while the best overall was for the SOWFA and JHU case, with a percent error at most turbines below 4%.

Next, we compare the distribution of the turbulence properties ($\mathcal{P}$=TKE, TI) for the three LES datasets, starting with the WRFLES suite, against those calculated with the KA2025 and QI2021 models for TKE and TI, respectively, under the superposition methods discussed in the framework (Figs. 5–6). Starting with TKE, the first row in Fig. 5 shows that the magnitude of TKE in the wake of the front-row wind turbine is lower than the TKE behind the second and third turbines for all three stability conditions, which suggests that TKE is slightly additive as more wakes overlap in a wind farm, at least in first three rows. This property is captured with the simple summation method, especially under unstable conditions; by contrast, the normalized method tends to incorrectly place the highest added TKE after the second turbine.

The maximum TKE occurs near the rotor tips ($y/D = \pm 0.5$) in this plane, which all methods captured properly. In addition, while the largest values of TKE are seen in unstable conditions, up to 3.2 $\mathrm{m^2 s^{-2}}$, the background TKE are also highest in unstable conditions (≈ 1 $\mathrm{m^2 s^{-2}}$), thus the TKE added by the turbines is ≈ 2.2 $\mathrm{m^2 s^{-2}}$. Similar amounts of added TKE are also found in neutral and stable conditions (Fig. 5, second and third columns).

A general feature that emerges from Figs. 5 and 6 is that the magnitude of added TKE and added TI in overlapping wakes is inversely proportional to the value of the m coefficient, i.e., it is highest for $m = 0.8$ and lowest for $m = 2$, for both superposition methods. Additionally, the SS method tends to add more TKE and TI than the NS method. As such, the selection of which wake superposition method to pick may depend on the performance of the analytical model associated with it: if the

https://doi.org/10.5194/wes-2025-220
Preprint. Discussion started: 14 November 2025

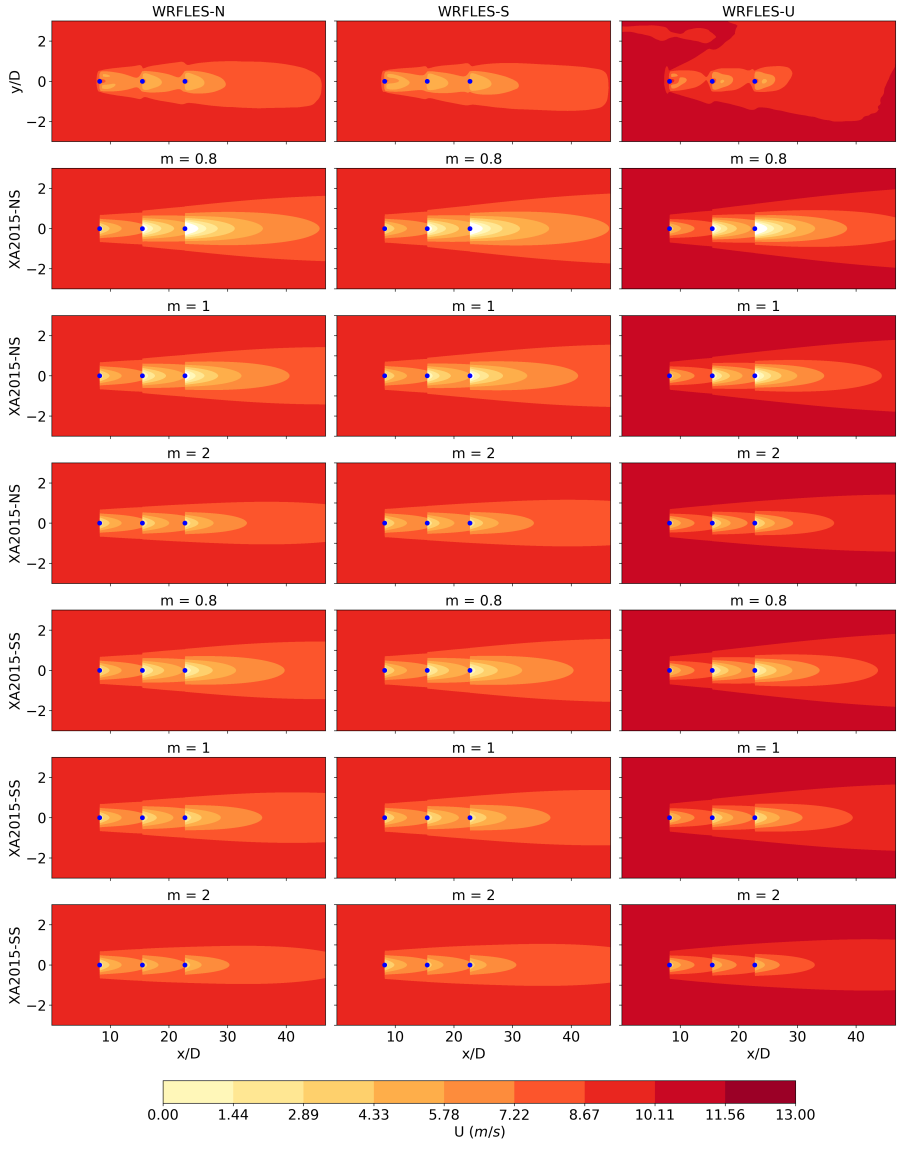

Figure 3. Contours of U by the XA2015 model (Eq. 3) with the NS superposition (XA2015-NS, Eq. 36) and the SS superposition (XA2015-SS, Eq. 37) for different values of m (0.8, 1, and 2) against the WRFLES results (WRFLES-N for neutral, WRFLES-S for stable, and WRFLES-U for unstable) at hub height in the $x-y$ plane. The blue dots represent the wind turbine locations in the domain.

analytical model generally underestimates the desired property, then a low value of m in conjunction with the simple method might deliver better results, and vice versa. In fact, the KA2025 model tends to produce a negative bias, thus underestimates added TKE (Khanjari et al., 2025), and, not surprisingly it performs best with the SS method and $m = 0.8$. By contrast, the

https://doi.org/10.5194/wes-2025-220
Preprint. Discussion started: 14 November 2025

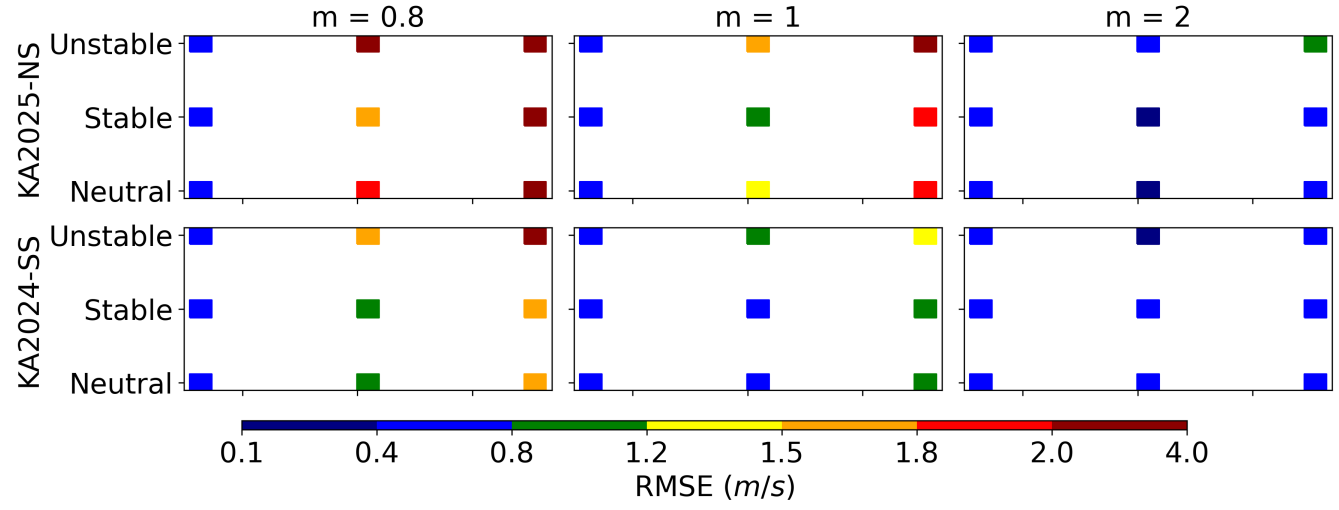

Figure 4. RMSE of wind speed calculated with the XA2015 model for the three WRFLES datasets utilized in this study.

QI2021 model tends to overestimate TI (i.e., positive bias) and therefore it performs best with a high value of m and with the NS method (Fig. 6).

Because the focus of this study is on TKE and because the general features of the two superposition methods are consistent for both turbulence properties, we are now going to discuss mostly TKE. The spanwise profiles downwind of each turbine at $x = 5D$ from the WRFLES-N case (Fig. 7) confirm that the SS method generates higher TKE than the NS method for the same value of m, but the best match occurs for m=1, especially at the second turbine. The profiles at the first turbine are collapsed into one, as there is no wake overlapping there. The NS method consistently underpredicts the wake TKE for all values of m. Similar patterns are also found for the stable and unstable WRFLES cases (Figs. A3 and A5).

In the vertical (Fig. 8), the general patterns of a TKE peak in the upper part of the rotor and a second weak peak at the lower part are well reconstructed by the KA2025 analytical model for all cases, but TKE drops too rapidly above the rotor. Again, higher values of m imply lower values of added TKE, especially for the normalized summation method. The $m = 0.8$ results with the simple summation method overestimate the peak TKE, thus the best performance is achieved with $m = 1$.

To assess the evolution of the wake TKE downstream, it is common practice in the literature (Delvaux et al., 2024; Risco et al., 2023) to calculate its average inside the rotor area at each grid point, centered at hub height, downstream of each wind turbine (called a "rotor-integrated" TKE). The WRFLES results in Fig. 9 show clearly the slightly additive nature of TKE, as the peaks of rotor-integrated TKE from the LES tend to increase after each additional turbine; this is also the case for TI (Fig. A7). As hinted earlier, the normalized summation method does not capture this feature well: for all the values of m, the peak is located at the second wind turbine, not the third. If this is an important characteristics to capture with the superposition method, then the simple summation is a better choice, especially with $m = 1$ or $m = 0.8$; however, with $m = 2$, also the simple summation method is inadequate.

https://doi.org/10.5194/wes-2025-220
Preprint. Discussion started: 14 November 2025

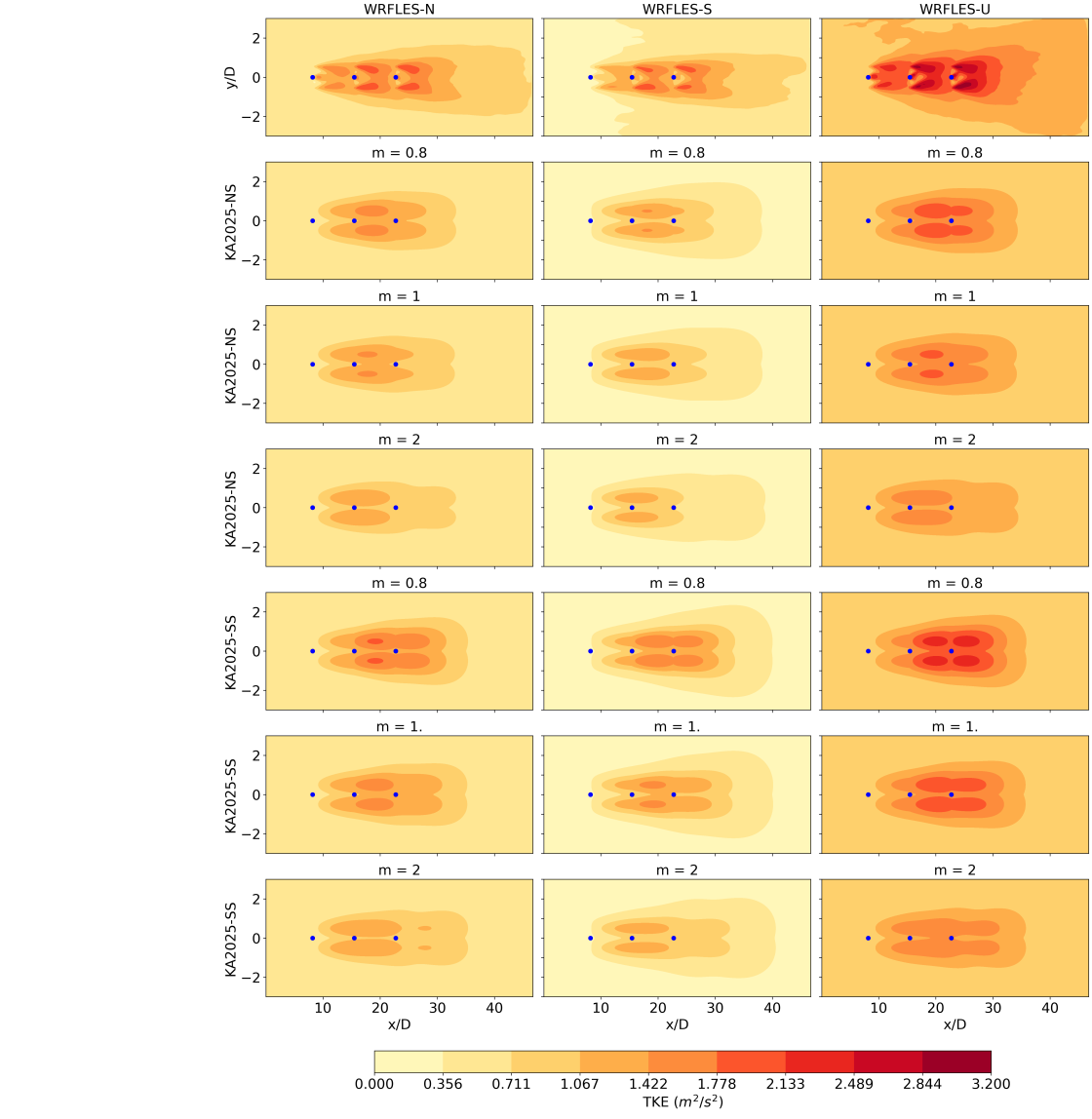

Figure 5. As in Fig. 3, but for TKE contours with KA2025-NS and KA2025-SS.

Focusing next on the JHU dataset (Fig. 10), which was obtained under neutral atmospheric conditions, it appears that the simulated column of wind turbines is characterized by rather strong turbulence, with a background value around 1.2 m^2s^{-2}, even higher than that in the WRFLES-U dataset. The wind turbines also contribute large amounts of TKE to the flow, with values greater than 5 m^2s^{-2} at several rotor tips. The added TKE by the first turbine is lower than that added by the rest of the turbines but it does not increase or decrease much after the seventh row. TKE is also high above the wind turbine column (not shown). These conditions are somewhat unusual. As a result, all superposition methods with the KA2025 model fail at

https://doi.org/10.5194/wes-2025-220
Preprint. Discussion started: 14 November 2025

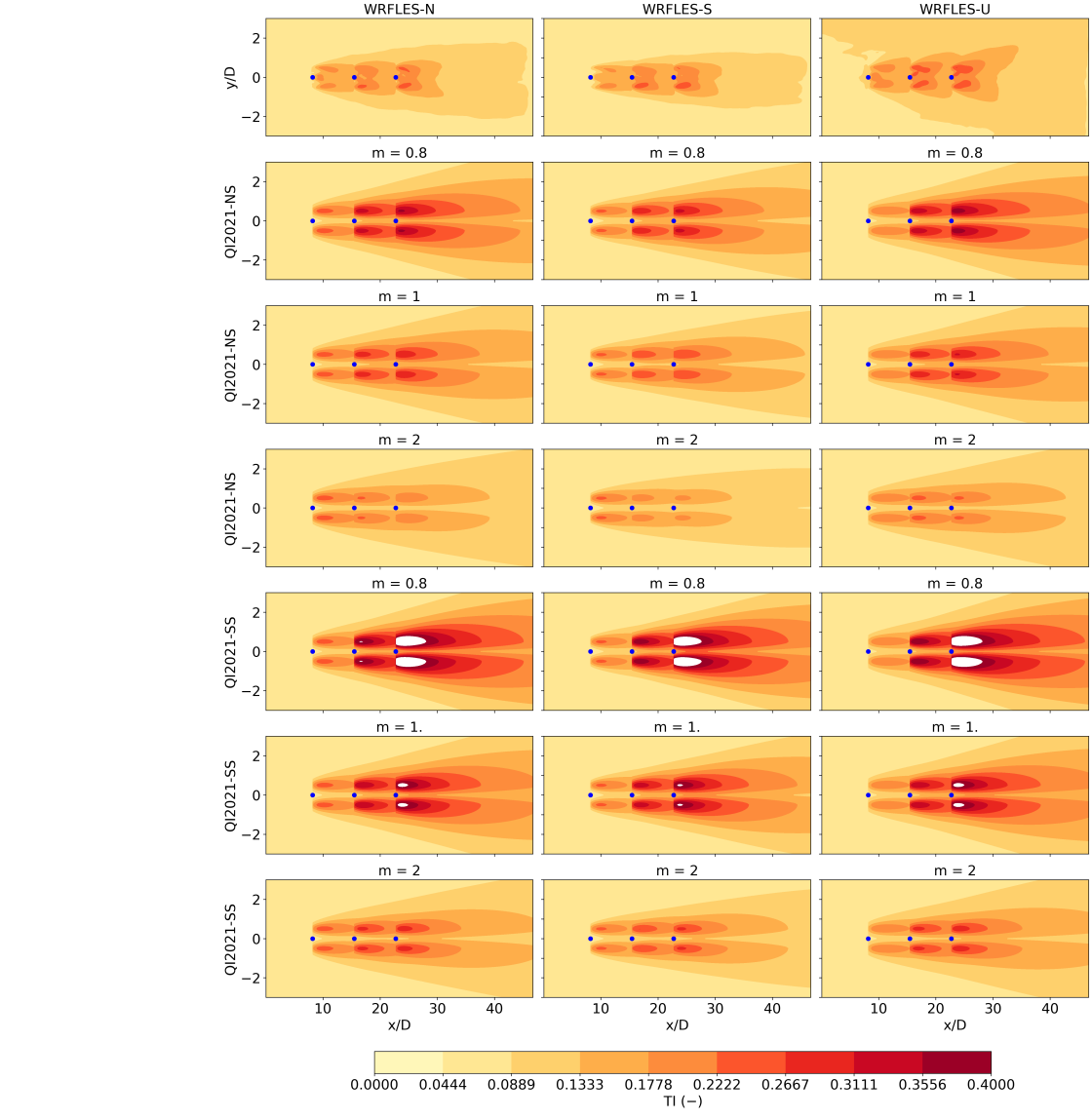

Figure 6. As in Fig. 5, but for TI contours with QI2021-NS and QI2021-SS. Values larger than 3.2 m^2s^{-2} are intentionally left blank to emphasize the overestimation.

reproducing such large amounts of TKE, especially above the rotors (Fig. 11), although the peaks in the vertical are relatively well captured, especially with the SS method with $m = 0.8$.

An important limitation of using a value of $m < 1$ (i.e., $m = 0.8$) is that, if $\Delta\mathcal{P}_i$ becomes negative for whatever reason, then the superposition cannot be calculated because a negative value cannot be raised to a power less than one. This is what may happen with added TI from the QI2021 method in Eq. 6: since the δz term is positive-defined and it is always subtracted from

https://doi.org/10.5194/wes-2025-220
Preprint. Discussion started: 14 November 2025

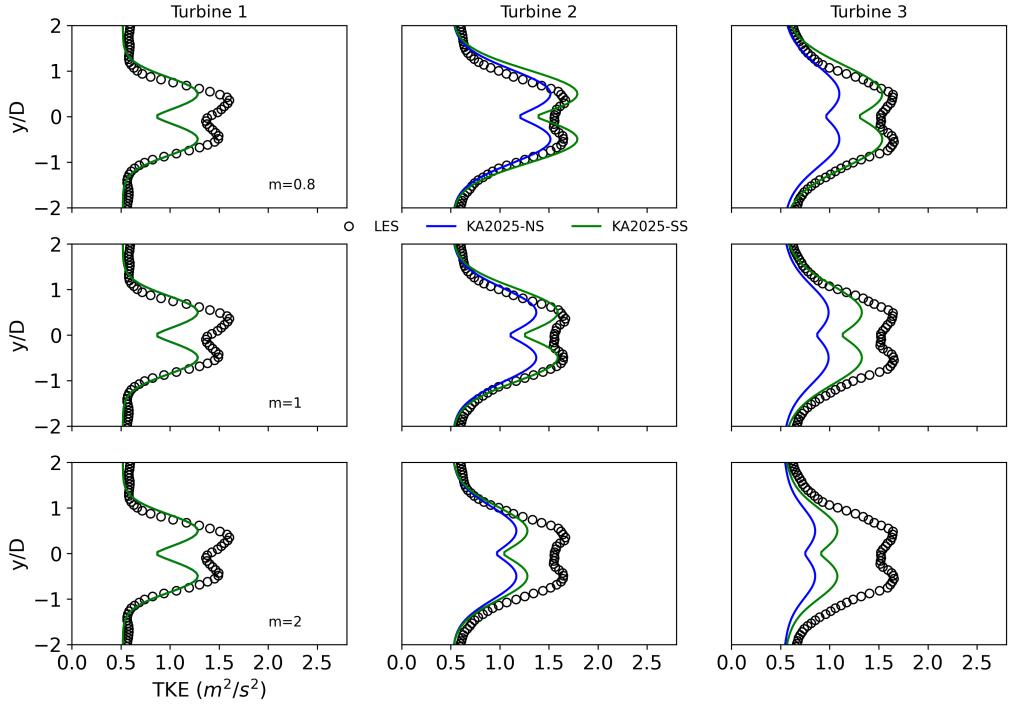

Figure 7. Profiles of TKE as a function of y at $z = H$ and $x = 5D$ from the KA2025 model with the two superposition methods for m = 0.8, 1, or 2 (on the first, second, and third row, respectively) against the WRFLES-N results for the three aligned wind turbines, one per column.

the background TI, it may cause not only negative values of ΔTI (Fig. A10) and possibly nonphysical negative values of TI, but also the failure of any superposition method based on $m < 1$. This failure can be appreciated in Fig. 12, top panel. With $m = 0.8$, the values of ΔTI below the rotor become negative starting at the third turbine and therefore the superposition cannot even be calculated for the remaining turbines. Above the rotor lower tip, where $\delta z = 0$, the NS method gives an excellent matching of the LES profiles, while the SS method produces unrealistically large values of added TI.

A different problem with the QI2021 analytical model emerges with $m = 1$ (Fig. 12, middle panel). The more turbines are in line, the larger the magnitude of negative ΔTI below the rotor from the δz term. With the SS method, this causes increasingly larger and unrealistic negative values of TI, literally off the charts; with the NS method, since the negative ΔTI is divided by a possibly negative TI_{in}, the ratio may become positive for some turbines and some locations, thus introducing the nonphysical zig-zag pattern shown in Fig. 12 (middle panel). With $m = 2$ (Fig. 12, bottom panel), the negative ΔTI is squared and therefore it introduces additional positive TI below the rotor, which gives rise to the nonphysical bump of high TI, noticeable from the fourth turbine.

https://doi.org/10.5194/wes-2025-220
Preprint. Discussion started: 14 November 2025

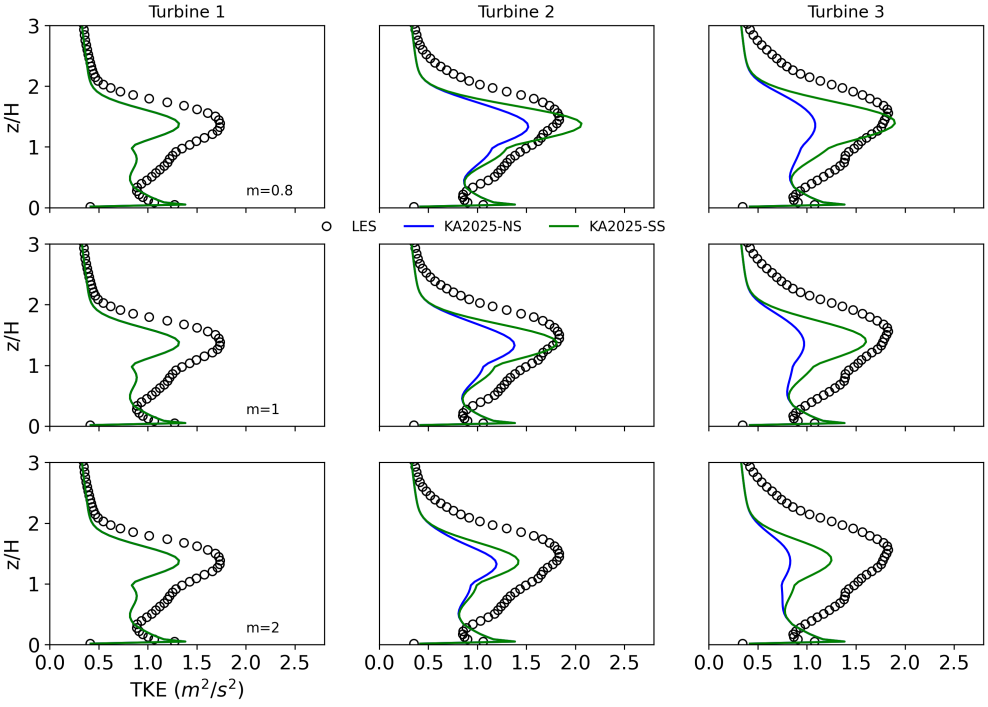

Figure 8. Same as Fig. 7, but for TKE as a function of z at $y = y_i$.

From a personal communication, the QI2021 authors recommended to follow IEC 61400-1 guidance (International Electrotechnical Commission, 2019, Eq. E.2) and set any added TI to zero after $10D$. With this modification, the vertical profiles of TI are indeed excellent (Fig. A11), especially with the NS method with $m = 2$. However, while this fix removes the unrealistic zig-zags and bump from the profiles at $5D$, it introduces a different problem: it causes unrealistic jumps in the distribution of both TI (Fig. A10) and rotor-integrated TI (Fig. A12). Ironically, the patterns of rotor-integrated TI are more than satisfactory with the original formulation (i.e., without the IEC 61400-1 fix) with the SS method, as shown in Fig. 13b, because the rotor-integrated TI is not affected by values below the rotor. However, some unrealistic features still exist with the NS method and $m = 1$.

The rotor-integrated TKE is generally underestimated with the KA2025 model (Fig. 13a), but the combination of the SS method with $m = 0.8$ performs best. With all superposition methods, the TKE peaks are approximately constant after the fourth turbine, as in the JHU LES results. This suggests that TKE is slightly additive only after a few turbines, and it eventually reaches a plateau.

Lastly, the performance of the superposition methods is evaluated with the SOWFA dataset, which may provide additional insights because the wind turbine columns are not aligned with the westerly wind direction (Fig. 14). Since the distance between

https://doi.org/10.5194/wes-2025-220
Preprint. Discussion started: 14 November 2025

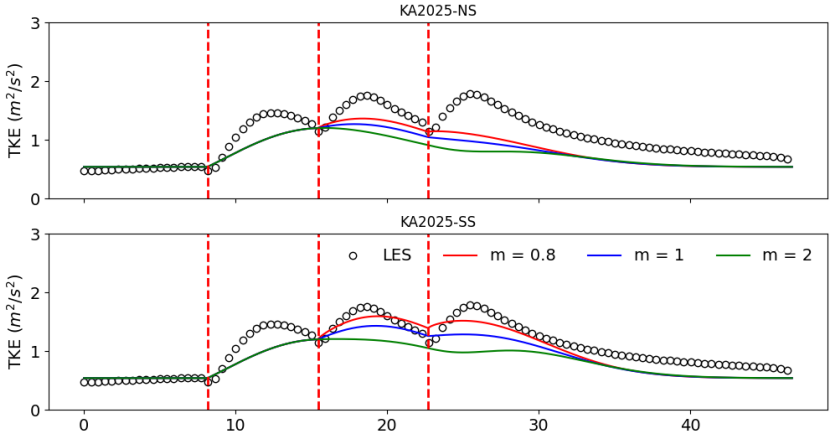

Figure 9. Rotor-integrated TKE as a function of downstream distance from the NS (top) and SS (bottom) methods against the WRFLES-N results.

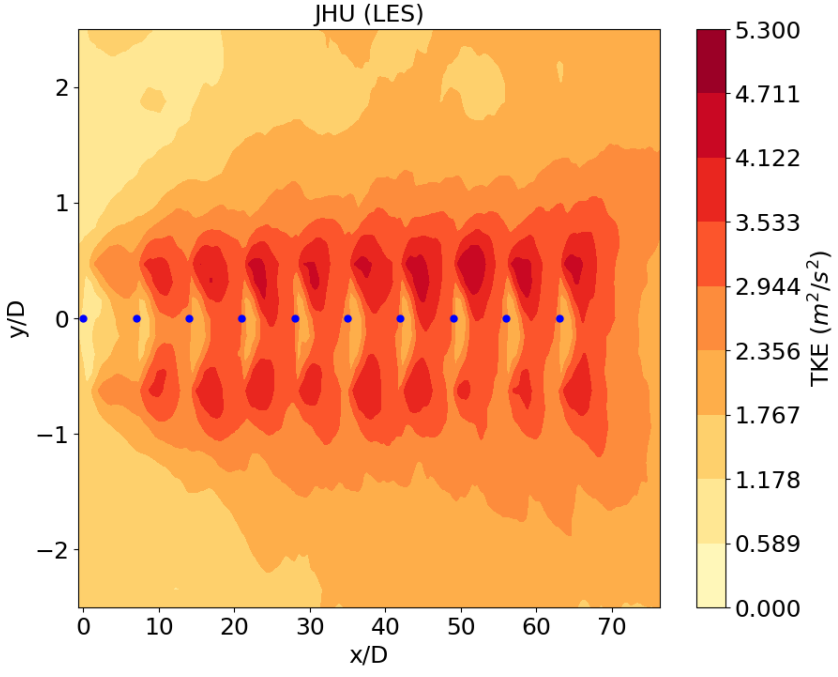

Figure 10. Contours of TKE at hub height in the $x - y$ plane from the JHU dataset.

https://doi.org/10.5194/wes-2025-220
Preprint. Discussion started: 14 November 2025

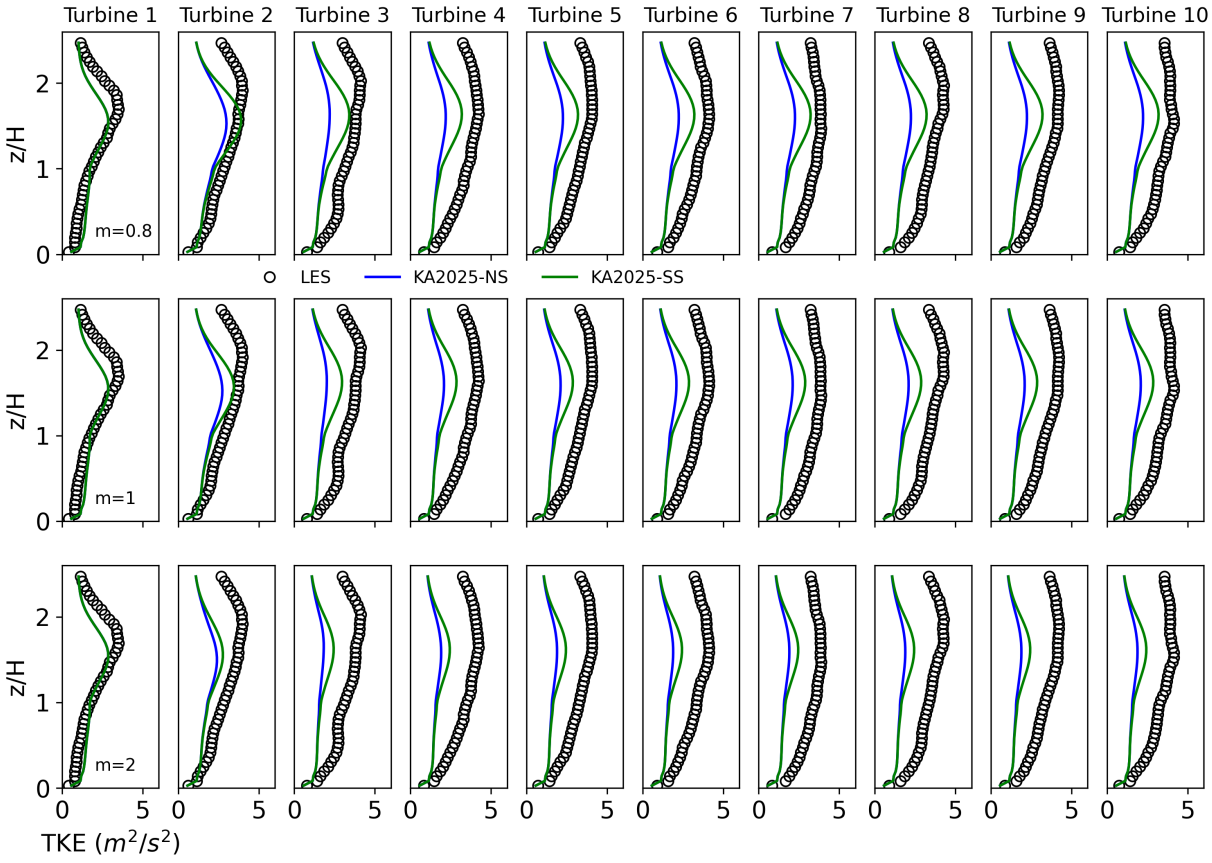

Figure 11. Profiles of TKE as a function of z at $y = y_i$ and $x = x_i + 5D$ from the KA2025 model with the two superposition methods for $m = \{0.8, 1, 2\}$ (on the first, second, and third row, respectively) against the JHU results for the ten aligned wind turbines, one per column.

turbines along the streamwise direction (x) is sufficiently large, the wake behind of each turbine can fully develop and extend well into the far-wake region. Additionally, some partial wake overlap is observed along the spanwise direction (y). The five turbines marked in red (named A-E) in Fig. 14 are analyzed in detail next.

Looking at the vertical profiles in Fig. 15, the pattern of higher TKE magnitude for smaller values of the m coefficient is less evident, possibly because the turbines in the A-E column are almost undisturbed, with the exception of a partial lateral wake overlap. The peaks of TKE profile (above the rotor tips with the LES and at the rotor tips with the KA2025 model) are underestimated, but the match below the rotor tip is excellent with the SS method, especially with $m = 0.8$. By contrast, the match between the analytical model and the LES results is poor above the rotor, where the KA2025 profiles grossly

https://doi.org/10.5194/wes-2025-220
Preprint. Discussion started: 14 November 2025

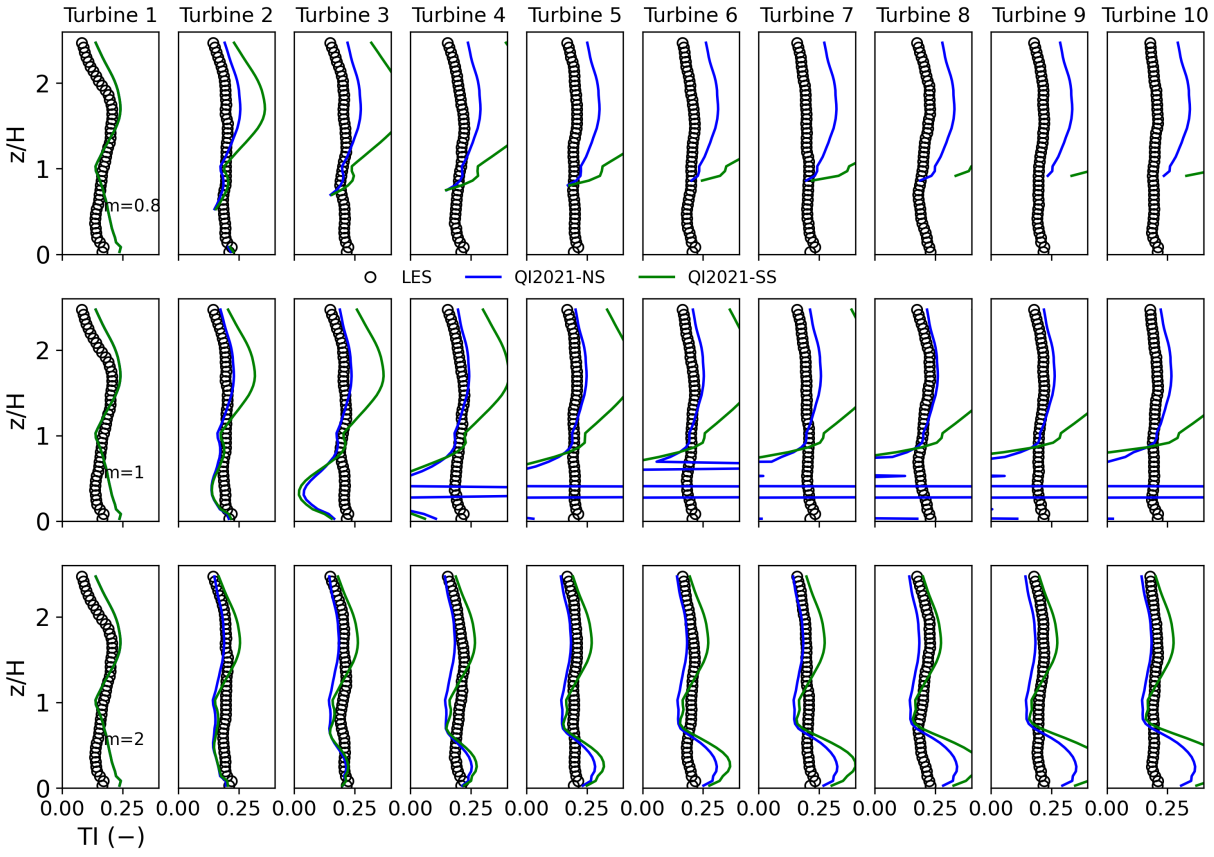

Figure 12. Same as Fig. 11, but for TI with QI2021.

underestimate TKE for all values of m, even for the first turbine A. This suggests that the KA2025 might need to be slightly re-tuned to better match the vertical TKE profiles above the rotor.

A spatial view of the performance of all superposition methods for all values of m and for all datasets is provided in Fig.16 for each wind turbine. The root-mean square error (RMSE) is calculated over the cylindrical volume of diameter equal to D centered at hub height with $1 < x/D < 7$ in the wake region of each turbine as follows:

$$RMSE = \sqrt{\frac{1}{n}\sum_{j=1}^{n}(TKE_{j,LES} - TKE_{j,KA2025})^2}, \tag{40}$$

where n is the number of grid points within the cylinder. The good performance of the KA2025 for a single turbine is evident from the very low RMSE of all the front-row turbines (<0.4 m^2 s^{-2} in all LES cases), especially with the JHU dataset (≈

https://doi.org/10.5194/wes-2025-220
Preprint. Discussion started: 14 November 2025

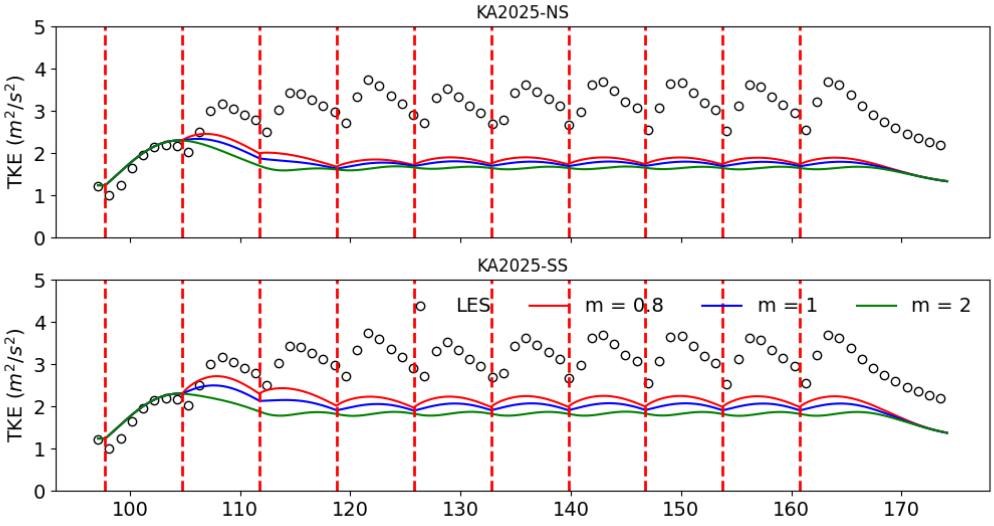

a)

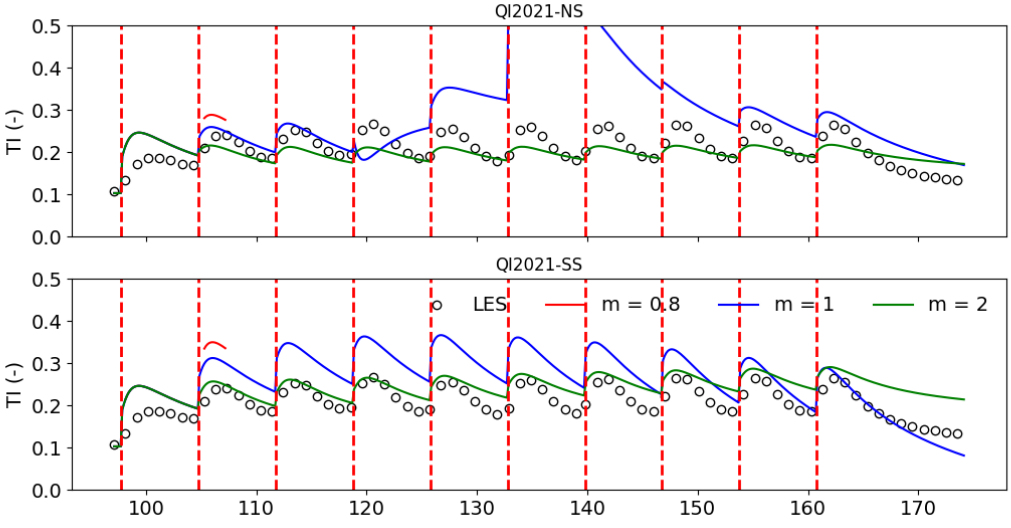

b)

Figure 13. As in Fig. 9, but for the JHU dataset with both the KA2025 model for TKE and the QI2021 model for TI.

0.1 m^2 s^{-2}). However, the JHU dataset has also the highest error for the inner turbines starting at the fourth row. Looking at the effect of atmospheric stability, the worst performance is for the unstable case (WRFLES-U), likely due to the inaccurate estimates of the hub-height inflow wind speed $U_{in,i}$ in that case (Fig. A2).

A summary of all cases, showing the average of the RMSE values of all the turbines, is provided in Table 2. For all cases, the RMSE is always lower with the SS than with the NS method for a given m. For the WRFLES and JHU cases, the RMSE is

https://doi.org/10.5194/wes-2025-220
Preprint. Discussion started: 14 November 2025

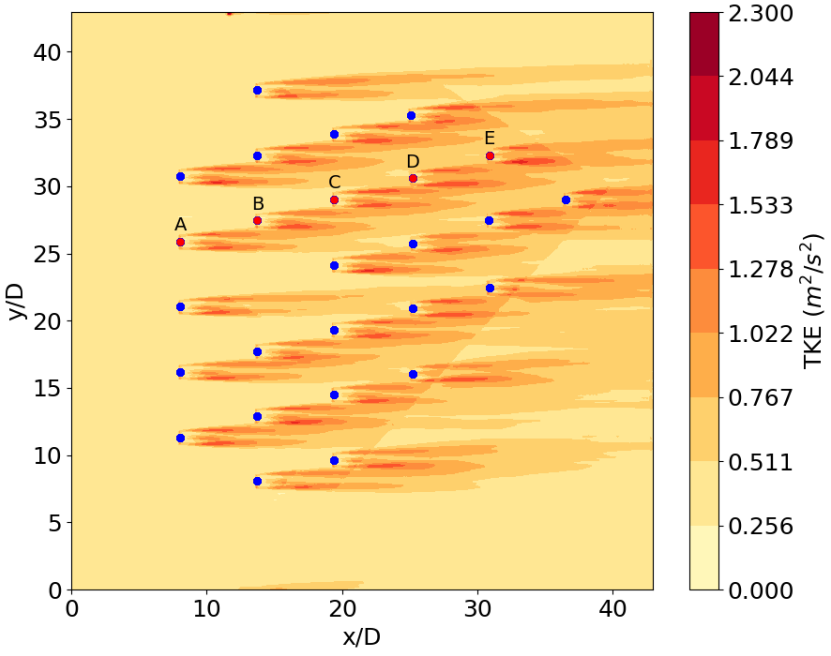

Figure 14. Contours of TKE at hub height in the $x-y$ plane from the SOWFA dataset. The column of wind turbines A-E will be evaluated next.

lowest with $m = 0.8$ for any given method. For the SOWFA case, the linear method ($m = 1$) with the SS performs better than the exponential method ($m = 0.8$).

Table 2. RMSE $[m^2/s^2]$ of the TKE superposition methods with the KA2025 model for the five LES cases considered in this study. The values in bold are the best for each LES case (i.e., each row).

LES case	Normalized summation (NS)			Simple summation (SS)		
	m = 0.8	m = 1	m = 1.2	m = 0.8	m = 1	m = 2
WRFLES-N	0.417	0.479	0.564	**0.300**	0.348	0.478
WRFLES-S	0.4527	0.509	0.5835	**0.247**	0.334	0.486
WRFLES-U	0.663	0.749	0.873	**0.516**	0.603	0.769
JHU	1.359	1.448	1.575	**1.073**	1.206	1.407
SOWFA	0.278	0.282	0.298	0.264	**0.247**	0.257

https://doi.org/10.5194/wes-2025-220
Preprint. Discussion started: 14 November 2025

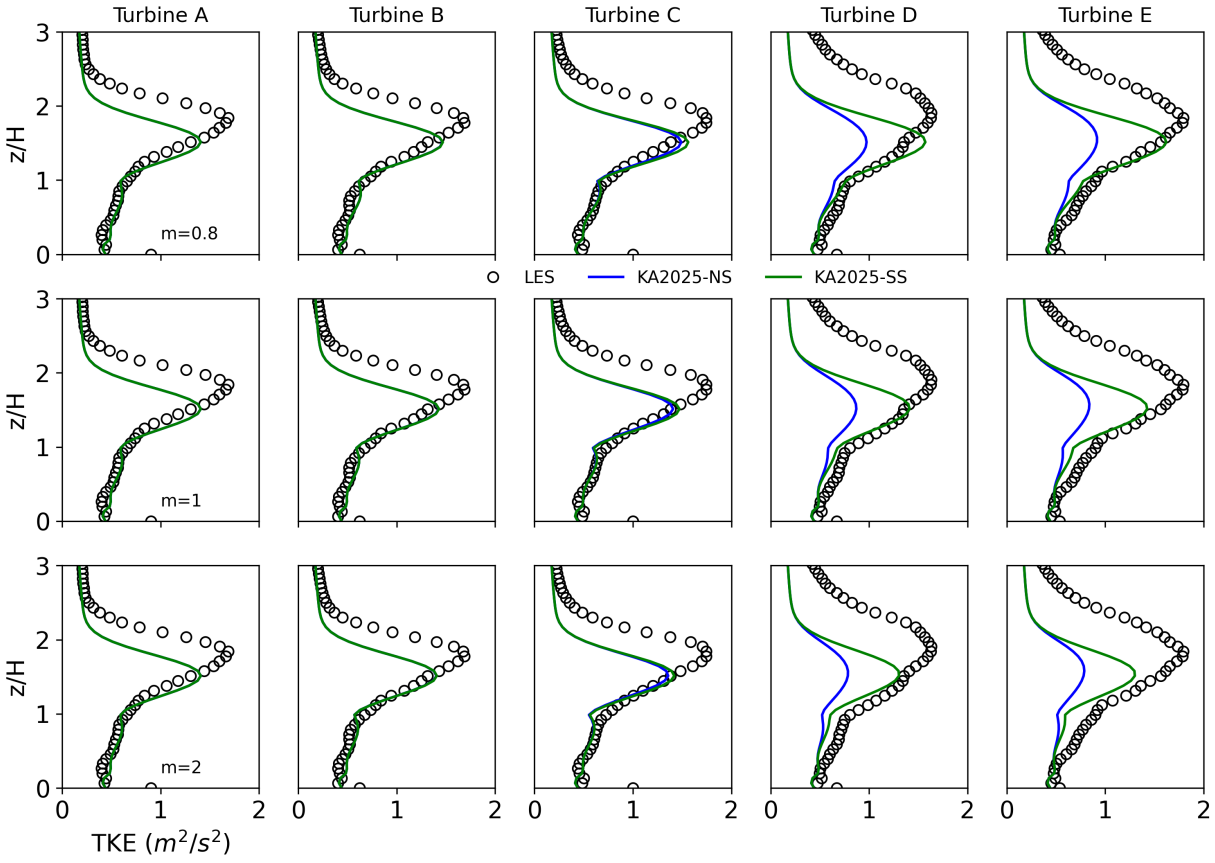

Figure 15. Same as Fig. 11, but the the five turbines A-E in the SOWFA dataset.

4 Conclusions and recommendations

In this study, we aimed to establish a comprehensive framework for investigating the superposition of any wake property $\mathcal{P}$, such as wind speed, turbulence intensity (TI), or turbulent kinetic energy (TKE), in a wind farm. The main focus was placed on TKE, which is an important variable in wind farm parameterizations (WFP) to account for turbulence generated by sub-grid turbine wakes in mesoscale models. Within the framework, two fundamental types of wake superposition methods were identified from the literature: simple summation (SS) and normalized summation (NS). The difference between the two is that the added wake property of interest is normalized by an upstream value in the NS method. With both methods, the value of an exponent (m) controls whether the summation is linear ($m = 1$), squared ($m = 2$), or exponential ($m = 0.8$). Basically, most wake superposition methods found in the literature can be simplified to one of these two types and those that differ are

https://doi.org/10.5194/wes-2025-220
Preprint. Discussion started: 14 November 2025

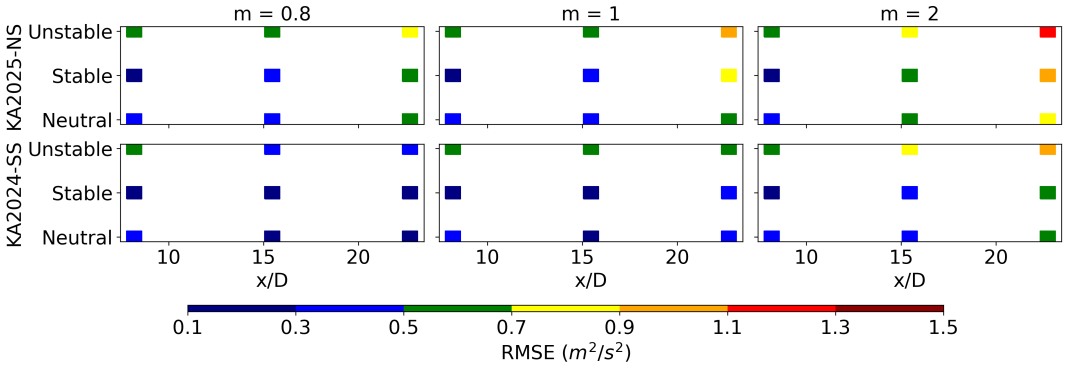

a)

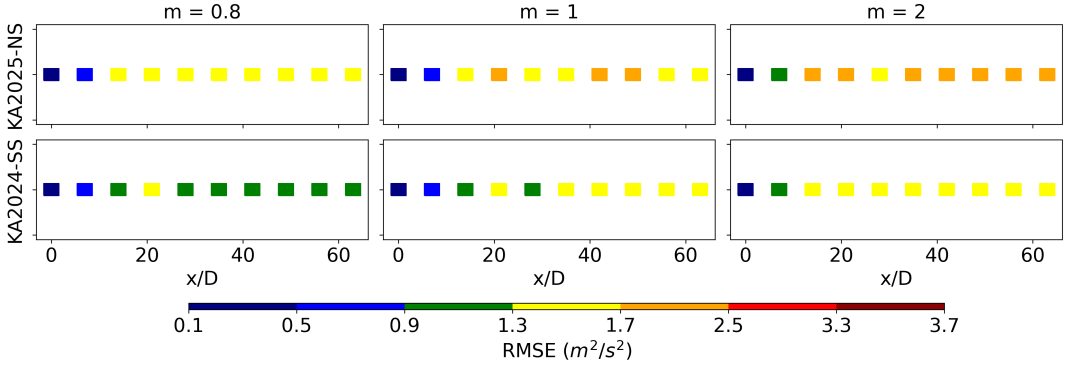

b)

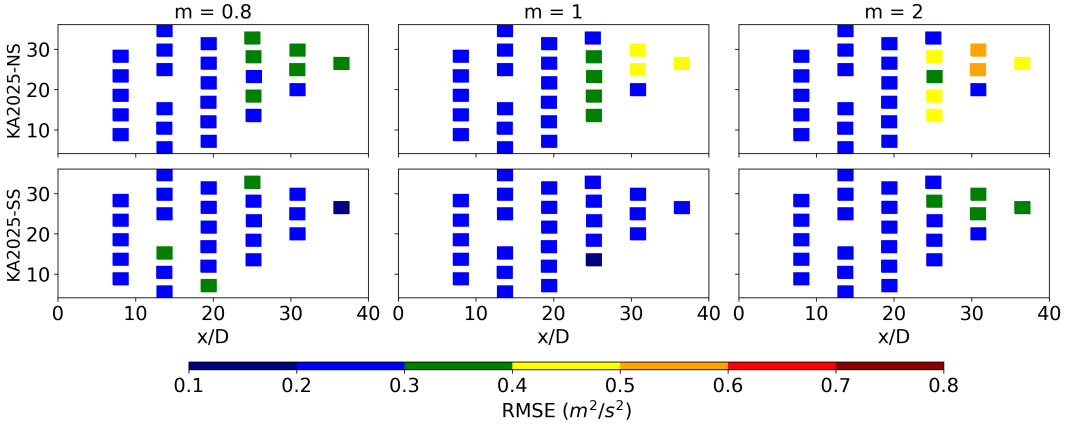

c)

Figure 16. RMSE $\left[m^2/s^2\right]$ of TKE superposition methods with the KA2025 model against the LES datasets: a) WRFLES, b) JHU, and c) SOWFA.

not suitable for implementation in WFPs for mesoscale models. The undisturbed wake property $\mathcal{P}_\infty$ can noticeably affect the calculations in both methods. As such, the first proposition of the framework is that the very concept of an undisturbed property, whether wind speed or turbulence, is not applicable to the majority of the turbines in a wind farm because only the front-row turbines experience it, while the rest are affected by a rather disturbed flow. A more general concept is that of an

https://doi.org/10.5194/wes-2025-220
Preprint. Discussion started: 14 November 2025

eawe european academy of wind energy
Open Access WIND ENERGY SCIENCE DISCUSSIONS

inflow property $\mathcal{P}_{in}$, which is the value of $\mathcal{P}$ at a fixed distance upstream. Thus, $\mathcal{P}_{\infty}$ is just a special case of $\mathcal{P}_{in}$ for the front row. The distance at which to obtain $\mathcal{P}_{in}$, which is the focus of the second proposition, needs to be clearly established and used consistently. Although here we use $-1D$, we recommend that the sensitivity of this choice be evaluated in future studies. In the third proposition, we recommend that $\mathcal{P}_{in}$ be a function of z, as opposed to being either a constant value at hub height or a rotor average. Especially with the NS method, without this assumption, the superposition methods fail at reconstructing the $\mathcal{P}$ distribution correctly.

Within this framework, we used three existing analytical models – XA2015 for normalized wind speed deficit, KA2025 for TKE, and QI2021 for TI – and compared their performance with both superposition methods and with all values of m against a suite of LES results from the existing literature: the stable, neutral, and unstable results from Wu et al. (2023) for three in-line wind turbines with WRFLES; the neutral LES of 10 in-line wind turbines from JHU; and the stable LES of a 48-turbine wind farm with SOWFA.

In general, we found that the SS methods tend to generate higher values of $\mathcal{P}$ than the NS methods. For example, the maximum value of added TI with $m = 1$ is up to 60% higher with SS than with NS for all stabilities in the WRFLES results. For the same superposition method, the coefficient m strongly controls the magnitude of the wake property, with the highest values for $m = 0.8$ in all cases analyzed here. For example, added TKE in the WRFLES results is up to 66% higher with $m = 0.8$ than with $m = 2$. Lastly, the SS methods are slightly additive, meaning that the wake property tends to increase with more in-line wind turbines. For example, the peaks of rotor-average added TKE in the WRFLES datasets are increasing from the first to the third turbine and only the SS methods could capture this behavior, while the NS methods produced a decrease of the peaks from the second to the third turbine. As such, the SS methods might be a better choice for additive properties like TI and TKE.

In general, the SS methods performed more reliably than NS methods, meaning that they were less likely to introduce spurious or nonphysical values. For example, for wind speed deficit, nonphysical negative values of wind speed right behind the turbine were found only with NS methods, especially in combination with $m < 1$. For added TI, the QI2021 formulation incorrectly introduced some negative values of turbulence intensity near the ground, which the NS methods then amplified via unrealistic vertical profiles of TI in overlapping wakes in all LES cases considered here. In fact, sometimes the RMSE or the actual wake profile could not even be calculated for the NS methods.

Consequently, the choice of superposition method and m value should depend on the bias of the analytical model. If the analytical model has a negative bias, as was the case with the KA2025 model that tends to underestimate TKE, the SS method is recommended with a lower m, whereas if the analytical model has a positive bias, like the QI2021 model that overestimates TI, a better agreement with the NS method and higher m is expected.

https://doi.org/10.5194/wes-2025-220
Preprint. Discussion started: 14 November 2025

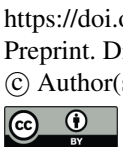

eawe european academy of wind energy
Open Access WIND ENERGY SCIENCE DISCUSSIONS

Appendix A: Supplemental figures

Appendix A contains additional figures that were briefly discussed in the main text.

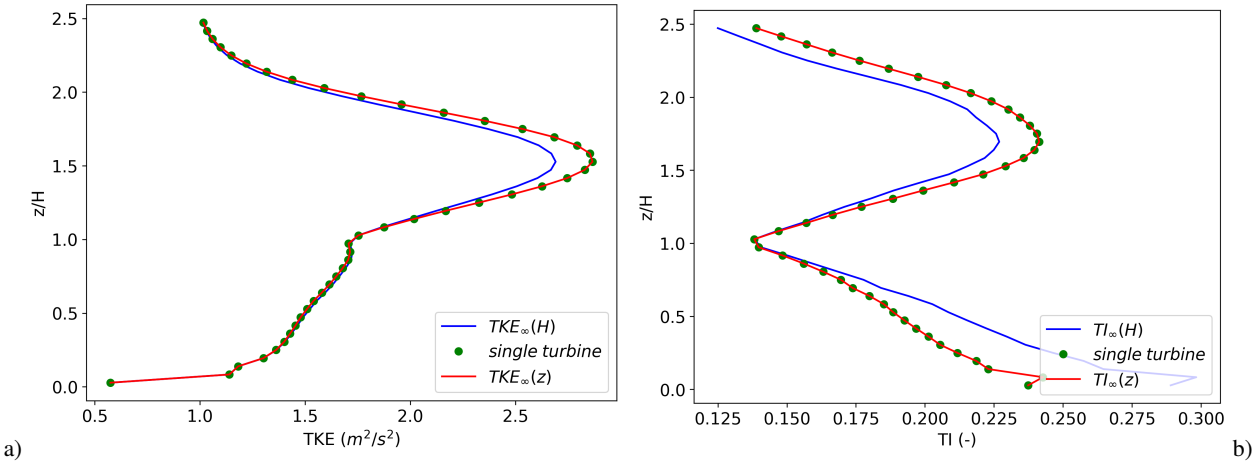

Figure A1. Error in the reconstruction of wake properties due to the constant inflow assumption: a) TKE with the KA2025 model and b) TI with the QI2021 method, both downstream of the first turbine at $x = 5D$. The three lines are the output of: the original analytical model for a single turbine (green circles), the output of the NS method for the front turbine with constant inflow (blue lines), and the output of the NS method for the front turbine with inflow varying with z (red line).

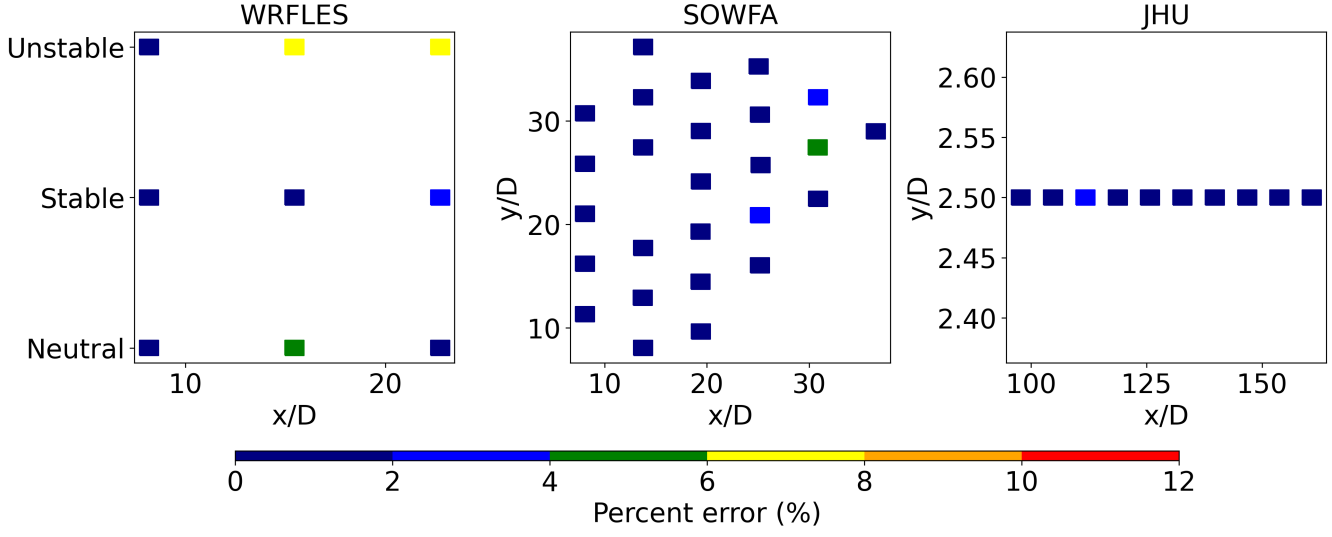

Figure A2. Percent error of inflow hub-height wind speed calculated with the XA model for the three LES datasets utilized in this study (Eq. 39).

https://doi.org/10.5194/wes-2025-220
Preprint. Discussion started: 14 November 2025

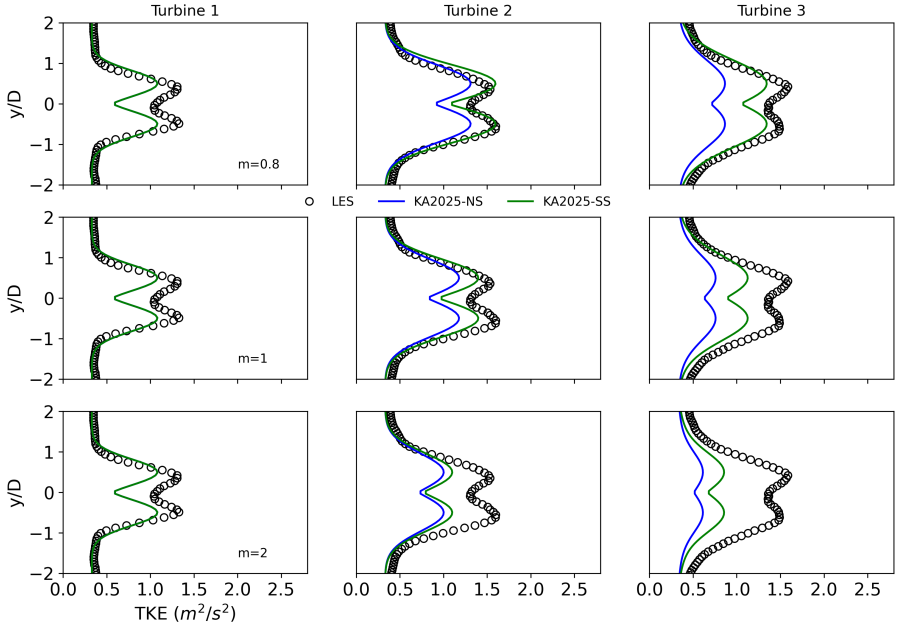

Figure A3. Same as Fig. 7, but against the WRFLES-S results.

https://doi.org/10.5194/wes-2025-220
Preprint. Discussion started: 14 November 2025

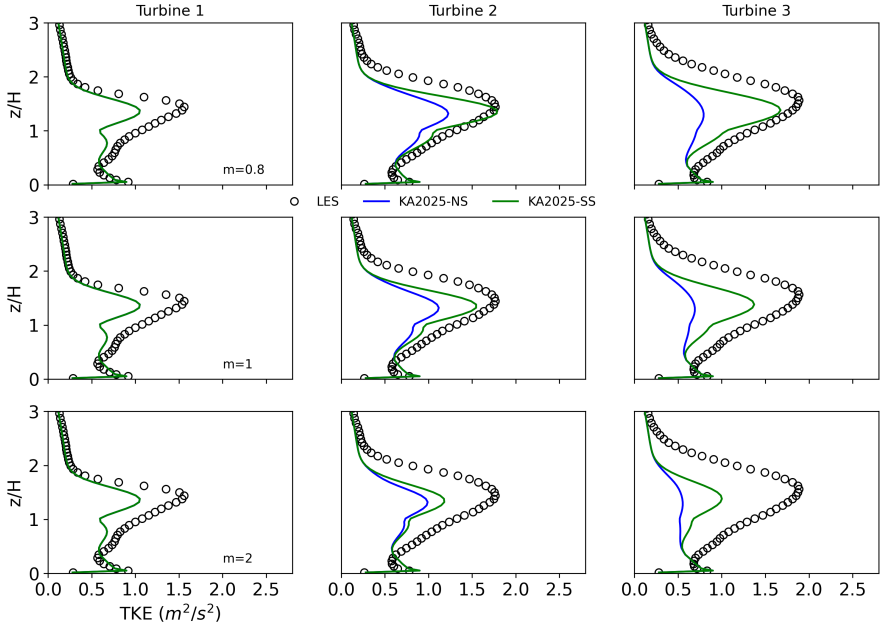

Figure A4. Same as Fig. 8, but against the WRFLES-S results.

https://doi.org/10.5194/wes-2025-220
Preprint. Discussion started: 14 November 2025

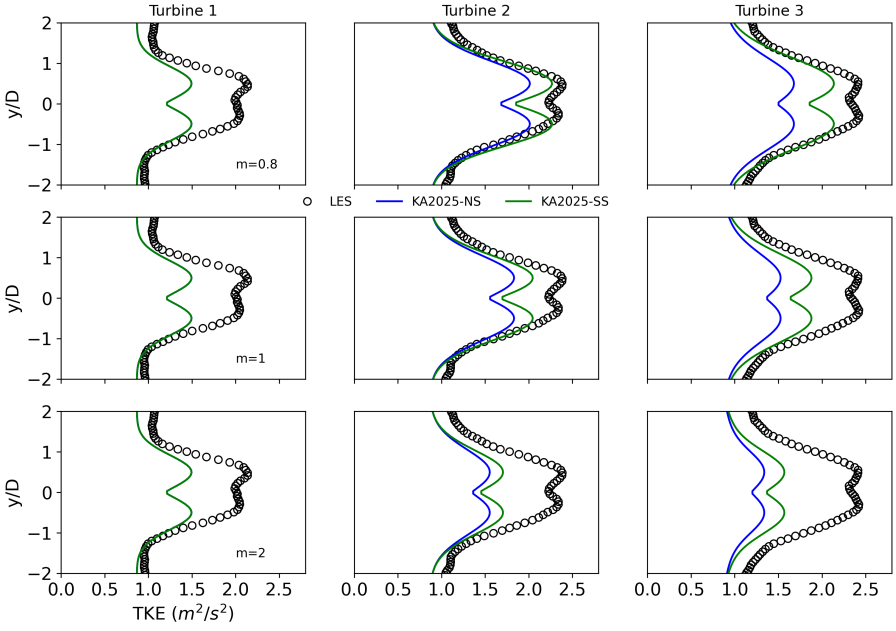

Figure A5. Same as Fig. 7, but against the WRFLES-U results.

https://doi.org/10.5194/wes-2025-220
Preprint. Discussion started: 14 November 2025

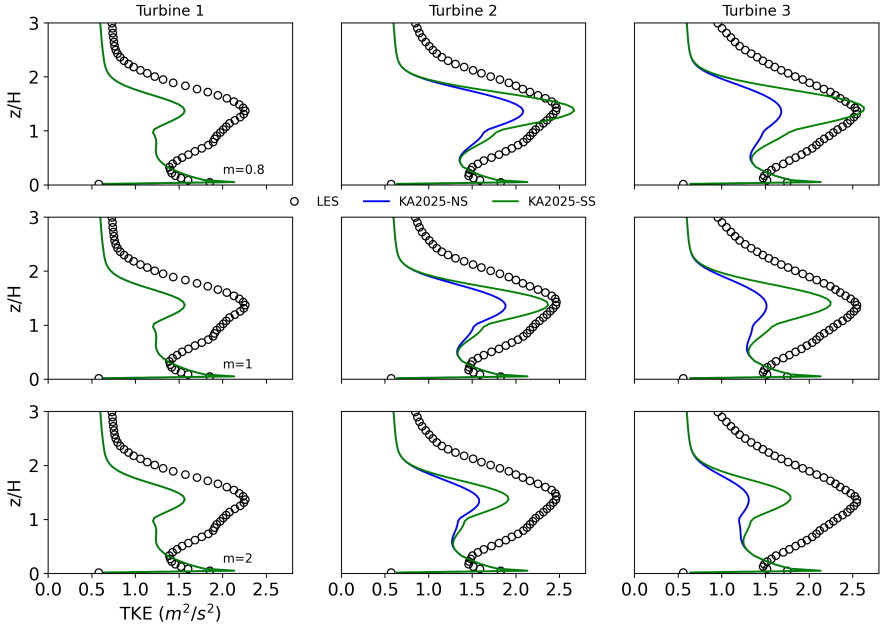

Figure A6. Same as Fig. 8, but against the WRFLES-U results.

https://doi.org/10.5194/wes-2025-220
Preprint. Discussion started: 14 November 2025

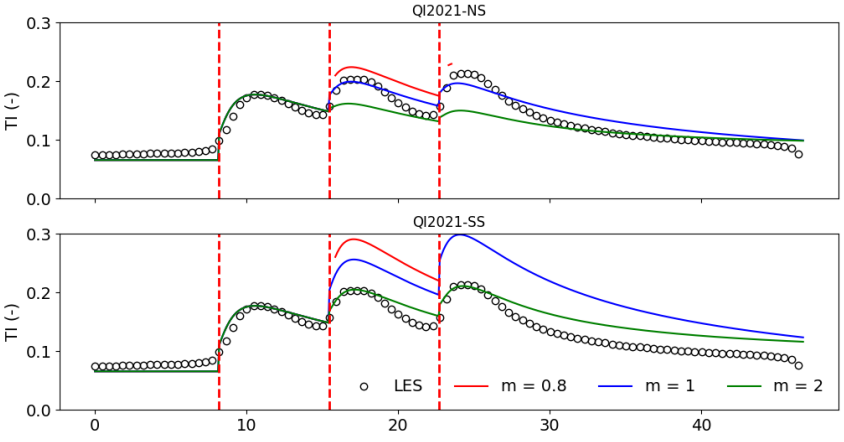

Figure A7. Same as Fig. 9, but for rotor-integrated TI calculated with the QI2021 method for the WRFLES-N case.

https://doi.org/10.5194/wes-2025-220
Preprint. Discussion started: 14 November 2025

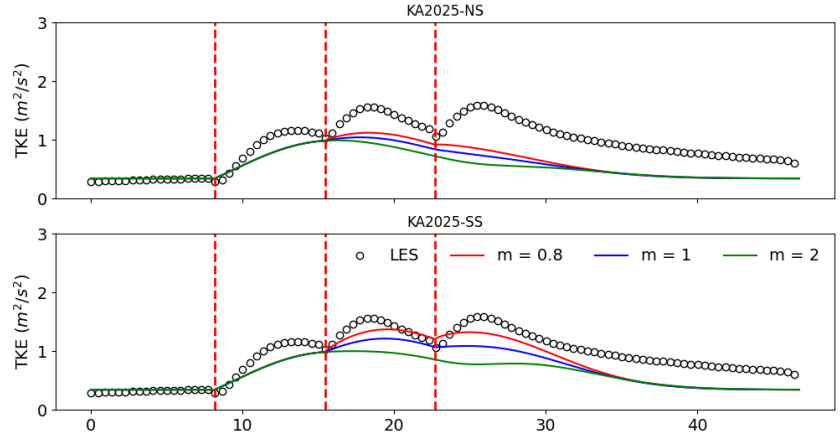

a)

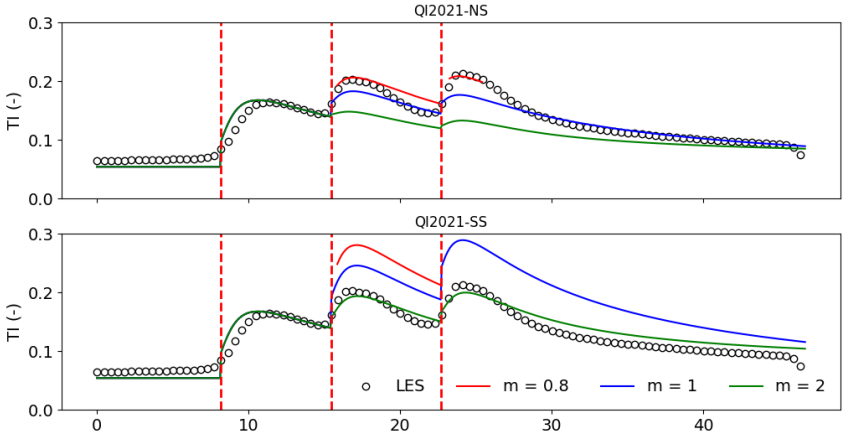

b)

Figure A8. The comparison of the average of TKE of superposition models with different amount of m against the results of WRFLES-S in the wake region.

https://doi.org/10.5194/wes-2025-220
Preprint. Discussion started: 14 November 2025

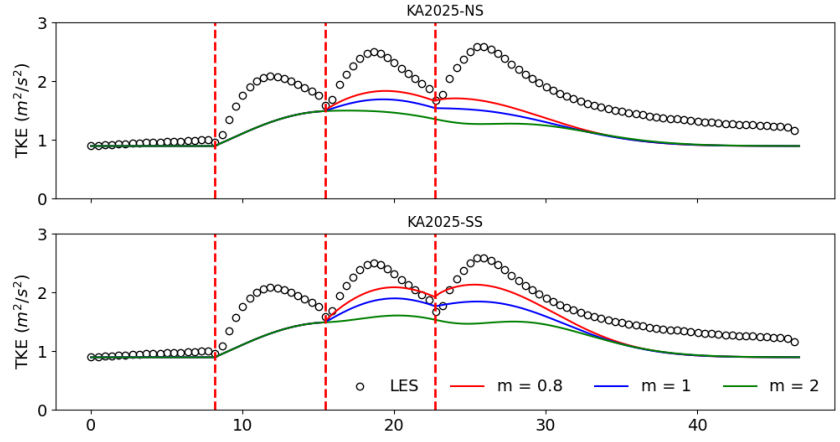

a)

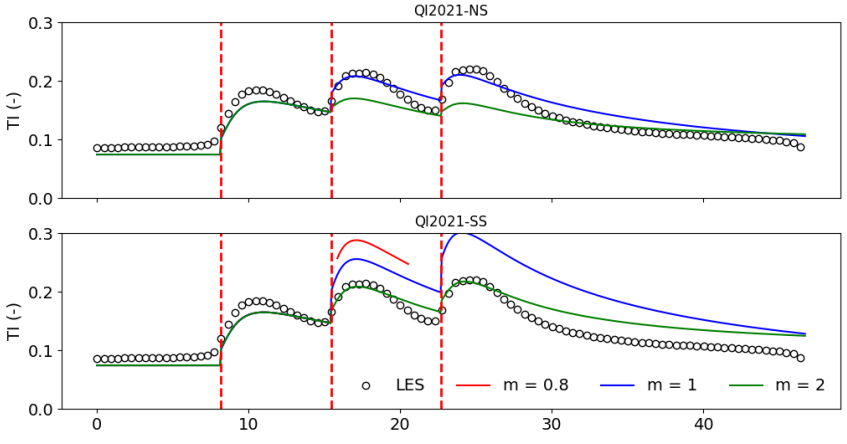

b)

Figure A9. The comparison of the average of TKE of superposition models with different amount of m against the results of WRFLES-U in the wake region.

https://doi.org/10.5194/wes-2025-220
Preprint. Discussion started: 14 November 2025

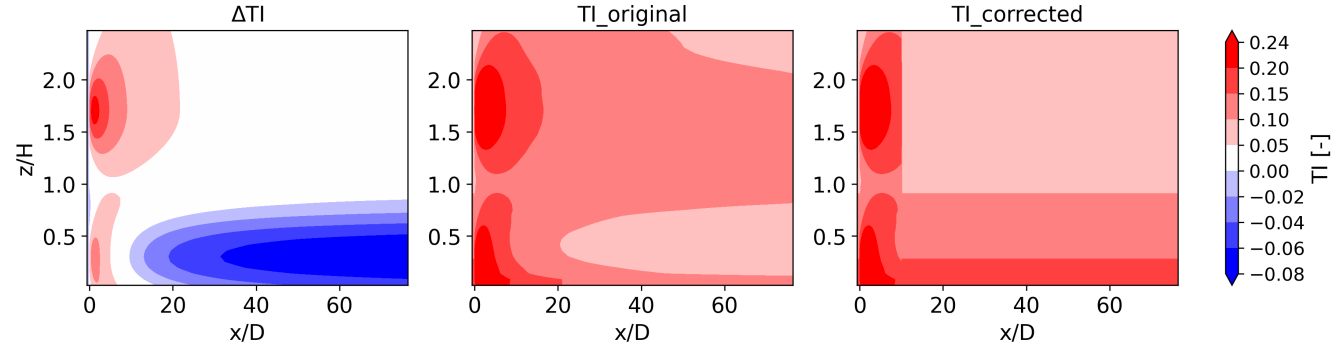

Figure A10. Added TI and total TI generated by the QI2021 model for a single wind turbine in the $x-z$ plane. If the δz term in Eq. 8 is set to zero after $10D$, the resulting unrealistic distribution of TI is shown in the right figure.

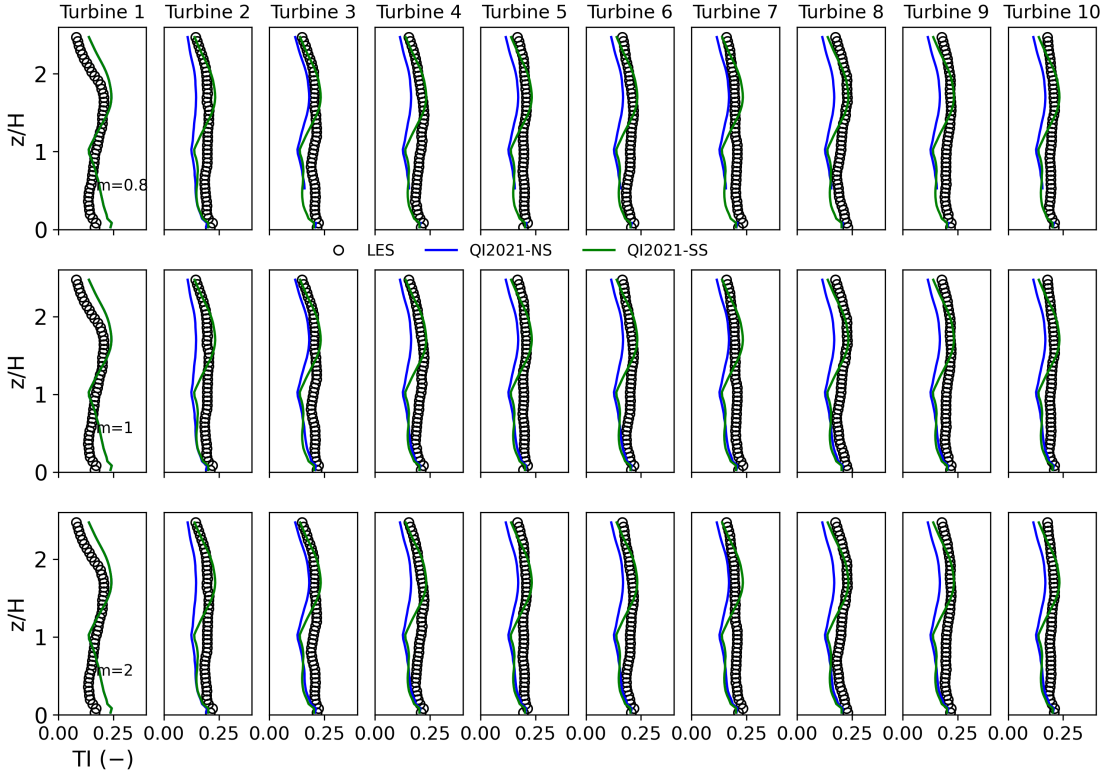

Figure A11. As in Fig. 12 but QI2021 is set to 0 beyond $10D$ of each turbine.

https://doi.org/10.5194/wes-2025-220
Preprint. Discussion started: 14 November 2025

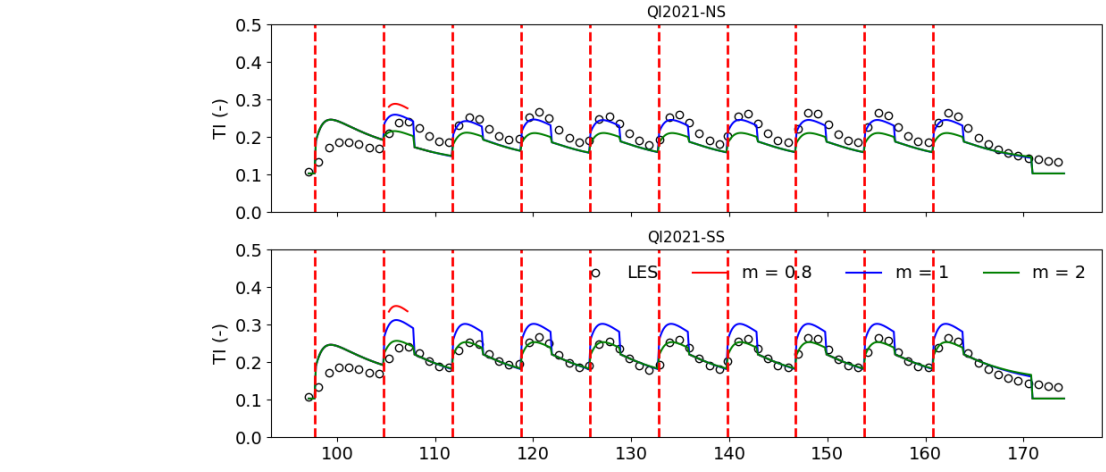

Figure A12. As in Fig. 13 but QI2021 is set to 0 beyond $10D$ of each turbine.

Code and data availability. N/A

Author contributions. Archer designed the research, obtained the funding, developed the formulation, and led the research; Khanjari led the Python coding and data processing; Archer and Khanjari analyzed the results and wrote the manuscript.

Competing interests. Archer is a member of the editorial board of Wind Energy Science.

Acknowledgements. This work was completed without any AI tools. The authors are grateful to the Johns Hopkins University team that made available the JHTDB-wind dataset and to Dr. Jason Jonkman of the U.S. National Renewable Energy Laboratory (NREL) for providing the thrust curve of the NREL 5 MW turbine.

https://doi.org/10.5194/wes-2025-220
Preprint. Discussion started: 14 November 2025

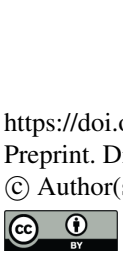

eawe european academy of wind energy
Open Access WIND ENERGY SCIENCE DISCUSSIONS

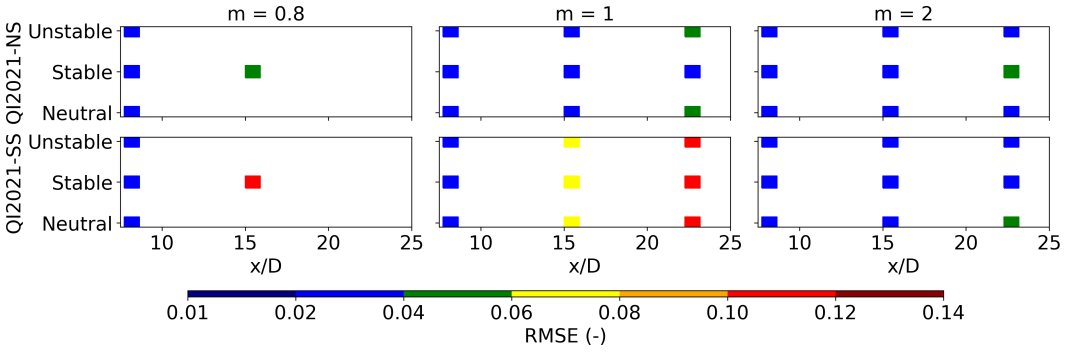

a)

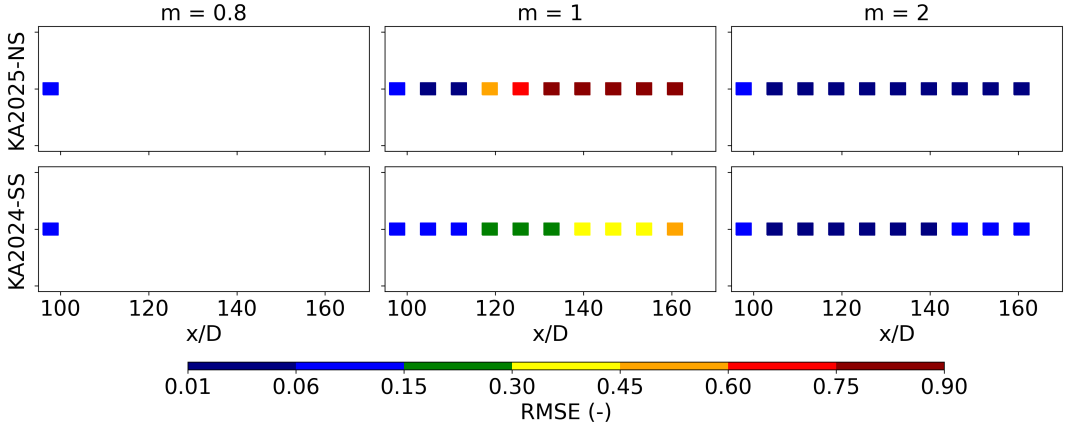

b)

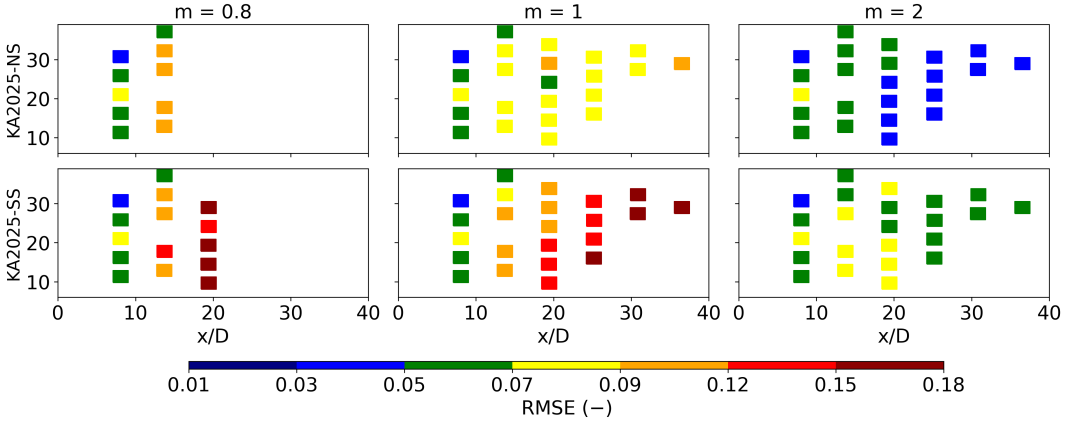

c)

Figure A13. As in Fig. 16 but for TI.

References

Abkar, M. and Porté-Agel, F.: A new wind-farm parameterization for large-scale atmospheric models, Journal of Renewable and Sustainable Energy, 7, 013 121, https://doi.org/10.1063/1.4907600, 2015.

https://doi.org/10.5194/wes-2025-220
Preprint. Discussion started: 14 November 2025

Archer, C. L.: Brief communication: A note on the variance of wind speed and turbulence intensity, Wind Energy Science, 10, 1433–1438, https://doi.org/10.5194/wes-2024-159, 2025.

Archer, C. L., Mirzaeisefat, S., and Lee, S.: Quantifying the sensitivity of wind farm performance to array layout options using large-eddy simulation, Geophysical Research Letters, 40, 4963–4970, https://doi.org/10.1002/grl.50911, 2013.

Archer, C. L., Vasel-Be-Hagh, A., Yan, C., Wu, S., Pan, Y., Brodie, J. F., and Maguire, A. E.: Review and evaluation of wake loss models for wind energy applications, Applied Energy, 226, 1187–1207, https://doi.org/10.1016/j.apenergy.2018.05.085, 2018.

Archer, C. L., Wu, S., Vasel-Be-Hagh, A., Brodie, J. F., Delgado, R., Pé, A. S., Oncley, S., and Semmer, S.: The VERTEX field campaign: Observations of near-ground effects of wind turbine wakes, Journal of Turbulence, 20, 64–92, https://doi.org/10.1080/14685248.2019.1572161, 2019.

Archer, C. L., Wu, S., Ma, Y., and Jiménez, P.: Two corrections for the treatment of turbulent kinetic energy in the WRF model, Monthly Weather Review, 148, 4823–4835, https://doi.org/10.1175/MWR-D-20-0097.1, 2020.

Barthelmie, R., Larsen, G., Pryor, S., Jørgensen, H., Bergström, H., Schlez, W., Rados, K., Lange, B., Vølund, P., Neckelmann, S., Mogensen, S., Schepers, G., Hegberg, T., Folkerts, L., and Magnusson, M.: ENDOW (Efficient Development of Offshore Wind Farms): Modelling wake and boundary layer interactions, Wind Energy, 7, 225–245, https://doi.org/10.1002/we.121, 2004.

Barthelmie, R. J., Hansen, K., Frandsen, S. T., Rathmann, O., Schepers, J., Schlez, W., Phillips, J., Rados, K., Zervos, A., Politis, E., et al.: Modelling and measuring flow and wind turbine wakes in large wind farms offshore, Wind Energy: An International Journal for Progress and Applications in Wind Power Conversion Technology, 12, 431–444, 2009.

Bastankhah, M. and Porté-Agel, F.: A new analytical model for wind-turbine wakes, Renewable Energy, 70, 116–123, https://doi.org/10.1016/j.renene.2014.01.002, 2014.

Bastankhah, M., Zunder, J. K., Hydon, P. E., Deebank, C., and Placidi, M.: Modelling turbulence in axisymmetric wakes: an application to wind turbine wakes, Journal of Fluid Mechanics, 1000, A2, 2024.

Bodini, N., Lundquist, J. K., and Kirincich, A.: US East Coast lidar measurements show offshore wind turbines will encounter very low atmospheric turbulence, Geophysical Research Letters, 46, 5582–5591, 2019.

Breton, S.-P., Sumner, J., Sørensen, J. N., Hansen, K. S., Sarmast, S., and Ivanell, S.: A survey of modelling methods for high-fidelity wind farm simulations using large eddy simulation, Philosophical Transactions of the Royal Society A: Mathematical, Physical and Engineering Sciences, 375, 20160 097, https://doi.org/10.1098/rsta.2016.0097, 2017.

Burton, T., Jenkins, N., Sharpe, D., and Bossanyi, E.: Wind energy handbook, John Wiley & Sons, 2011.

Churchfield, M., Lee, S., Moriarty, P., Martínez, L., Leonardi, S., Vijayakumar, G., and Brasseur, J.: Large-eddy simulations of wind-plant aerodynamics, pp. 1–19, 50th AIAA Aerospace Sciences Meeting, Nashville (Tennessee), 2012.

Crespo, A. and Hernández, J.: Turbulence characteristics in wind-turbine wakes, Journal of Wind Engineering and Industrial Aerodynamics, 61, 71–85, https://doi.org/10.1016/0167-6105(95)00033-X, 1996.

Delvaux, T., van der Laan, M. P., and Terrapon, V. E.: A new RANS-based added turbulence intensity model for wind-farm flow modelling, Journal of Physics: Conference Series, 2767, 092 089, https://doi.org/10.1088/1742-6596/2767/9/092089, 2024.

Díaz, H. and Soares, C. G.: Review of the current status, technology and future trends of offshore wind farms, Ocean Engineering, 209, 107 381, 2020.

Emeis, S.: Wind energy meteorology: atmospheric physics for wind power generation, Springer, 2018.

https://doi.org/10.5194/wes-2025-220
Preprint. Discussion started: 14 November 2025

Eriksson, O., Lindvall, J., Breton, S.-P., and Ivanell, S.: Wake downstream of the Lillgrund wind farm - A Comparison between LES using the actuator disc method and a wind farm parametrization in WRF, Journal of Physics: Conference Series, 625, 012 028, https://doi.org/10.1088/1742-6596/625/1/012028, 2015.

Fischereit, J., Brown, R., Larsén, X. G., Badger, J., and Hawkes, G.: Review of mesoscale wind-farm parametrizations and their applications, Boundary-Layer Meteorology, 182, 175—224, https://doi.org/10.1007/s10546-021-00652-y, 2022.

Fitch, A. C., Olson, J. B., Lundquist, J. K., Dudhia, J., Gupta, A. K., Michalakes, J., and Barstad, I.: Local and mesoscale impacts of wind farms as parameterized in a mesoscale NWP model, Monthly Weather Review, 140, 3017 – 3038, https://doi.org/10.1175/MWR-D-11-00352.1, 2012.

Frandsen, S., Barthelmie, R., Pryor, S., Rathmann, O., Larsen, S., Højstrup, J., and Thøgersen, M.: Analytical modelling of wind speed deficit in large offshore wind farms, Wind Energy, 9, 39–53, https://doi.org/10.1002/we.189, 2006.

Ghaisas, N. S., Archer, C. L., Xie, S., Wu, S., and Maguire, E.: Evaluation of layout and atmospheric stability effects in wind farms using large-eddy simulation, Wind Energy, 20, 1227–1240, https://doi.org/10.1002/we.2091, 2017.

Golbazi, M., Archer, C. L., and Alessandrini, S.: Surface impacts of large offshore wind farms, Environmental Research Letters, 17, 064 021, https://doi.org/10.1088/1748-9326/ac6e49, 2022.

International Electrotechnical Commission: Wind energy generation systems - Part 1: Design requirements, Tech. Rep. IEC 61400-1 Ed. 4.0 B:2019, IEC, Denmark, https://webstore.ansi.org/standards/iec/iec61400ed2019-2419167?source=blog, 2019.

Ishihara, T. and Qian, G.-W.: A new Gaussian-based analytical wake model for wind turbines considering ambient turbulence intensities and thrust coefficient effects, Journal of Wind Engineering and Industrial Aerodynamics, 177, 275–292, https://doi.org/10.1016/j.jweia.2018.04.010, 2018.

Jensen, N. O.: A note on wind generator interaction, Tech. Rep. Risø-M-2411, Risø National Laboratory, Denmark, 1983.

Johns Hopkins University: JHU Turbulence Database: Wind Farm – Neutral Case, https://turbulence.idies.jhu.edu/datasets/windfarms/neutralWindfarm, accessed: 2025-06-21, 2025.

Katic, I., Højstrup, J., and Jensen, N. O.: A simple model for cluster efficiency, pp. 407–410, European Wind Energy Association Conference and Exhibition (EWEC'86), Rome, 1986.

Khanjari, A., Feroz, A., and Archer, C. L.: An analytical formulation for turbulence kinetic energy added by wind turbines based on large-eddy simulation, Wind Energy Science, 10, 887–905, https://doi.org/10.5194/wes-10-887-2025, 2025.

Kumer, V.-M., Reuder, J., Dorninger, M., Zauner, R., and Grubišić, V.: Turbulent kinetic energy estimates from profiling wind LiDAR measurements and their potential for wind energy applications, Renewable Energy, 99, 898–910, 2016.

Larsen, G. C.: A simple wake calculation procedure, Tech. Rep. Risø-M-2760, Risø National Laboratory, Denmark, 1988.

Li, L., Huang, Z., Ge, M., and Zhang, Q.: A novel three-dimensional analytical model of the added streamwise turbulence intensity for wind-turbine wakes, Energy, 238, 121 806, https://doi.org/10.1016/j.energy.2021.121806, 2022.

Li, L., Wang, B., Ge, M., Huang, Z., Li, X., and Liu, Y.: A novel superposition method for streamwise turbulence intensity of wind-turbine wakes, Energy, 276, 127 491, 2023.

Lissaman, P. B. S.: Energy effectiveness of arbitrary arrays of wind turbines, Journal of Energy, 3, 323–328, https://doi.org/10.2514/3.62441, 1979.

Ma, Y., Archer, C. L., and Vasel-Be-Hagh, A.: Comparison of individual versus ensemble wind farm parameterizations inclusive of sub-grid wakes for the WRF model, Wind Energy, 25, 1573–1595, https://doi.org/10.1002/we.2758, 2022a.

https://doi.org/10.5194/wes-2025-220
Preprint. Discussion started: 14 November 2025

Ma, Y., Archer, C. L., and Vasel-Be-Hagh, A.: The Jensen wind farm parameterization, Wind Energy Science, 7, 2407–2431, https://doi.org/10.5194/wes-7-2407-2022, 2022b.

Madsen, H. A.: A CFD analysis of the actuator disc flow compared with momentum theory results, in: Proceedings of the 10th Symposium on Aerodynamics of Wind Turbines, pp. 109–124, IEA Joint Action, 1996.

Medici, D., Ivanell, S., Dahlberg, J.-r., and Alfredsson, P. H.: The upstream flow of a wind turbine: blockage effect, Wind Energy, 14, 691–697, https://doi.org/https://doi.org/10.1002/we.451, 2011.

Mikkelsen, R. F.: Actuator disc methods applied to wind turbines, Phd thesis, Technical University of Denmark, (DTU), mEK-FM-PHD No. 2003-02, 2003.

Mirocha, J. D., Kosovic, B., Aitken, M. L., and Lundquist, J. K.: Implementation of a generalized actuator disk wind turbine model into the Weather Research and Forecasting model for large-eddy simulation applications, Journal of Renewable and Sustainable Energy, 6, 013 104, https://doi.org/10.1063/1.4861061, 2014.

Morales, A., Wächter, M., and Peinke, J.: Characterization of wind turbulence by higher-order statistics, Wind Energy, 15, 391–406, 2012.

Nygaard, N. G.: Wakes in very large wind farms and the effect of neighbouring wind farms, Journal of Physics: Conference Series, 524, 012 162, https://doi.org/10.1088/1742-6596/524/1/012162, 2014.

Pan, Y. and Archer, C. L.: A hybrid wind-farm parametrization for mesoscale and climate models, Boundary-Layer Meteorology, 168, 469–495, https://doi.org/10.1007/s10546-018-0351-9, 2018.

Platis, A., Siedersleben, S. K., Bange, J., Lampert, A., Bärfuss, K., Hankers, R., Cañadillas, B., Foreman, R., Schulz-Stellenfleth, J., Djath, B., et al.: First in situ evidence of wakes in the far field behind offshore wind farms, Scientific reports, 8, 2163, 2018.

Porté-Agel, F., Bastankhah, M., and Shamsoddin, S.: Wind-turbine and wind-farm flows: a review, Boundary-layer meteorology, 174, 1–59, 2020.

Qian, G.-W. and Ishihara, T.: Wind farm power maximization through wake steering with a new multiple wake model for prediction of turbulence intensity, Energy, 220, 119 680, 2021.

Quarton, D. and Ainslie, J.: Turbulence in wind turbine wakes, Wind Engineering, 14, 15–23, 1990.

Risco, J. C., van der Laan, M., Pedersen, M., Forsting, A. M., and Réthoré, P.-E.: A RANS-based surrogate model for simulating wind turbine interaction, in: Journal of Physics: Conference Series, vol. 2505, p. 012016, IOP Publishing, 2023.

Schmitz, S.: XTurb-PSU: a wind turbine design and analysis tool, The Pennsylvania State University, 2012.

Siedersleben, S., Platis, A., Lundquist, J., Djath, B., Lampert, A., Bärfuss, K., Cañadillas, B., Schulz-Stellenfleth, J., Bange, J., Neumann, T., and Emeis, S.: Turbulent kinetic energy over large offshore wind farms observed and simulated by the mesoscale model WRF (3.8.1), Geoscientific Model Development, 13, 249–268, https://doi.org/10.5194/gmd-13-249-2020, 2020.

Simley, E., Angelou, N., Mikkelsen, T., Sjöholm, M., Mann, J., and Pao, L. Y.: Characterization of wind velocities in the upstream induction zone of a wind turbine using scanning continuous-wave lidars, Journal of Renewable and Sustainable Energy, 8, 013 301, https://doi.org/10.1063/1.4940025, 2016.

Skamarock, W. C., Klemp, J. B., Dudhia, J., Gill, D. O., Liu, Z., Berner, J., Wang, W., Powers, J. G., Duda, M. G., Barker, D., and Huang, X.-y.: A description of the Advanced Research WRF Model Version 4.3, Tech. rep., National Center for Atmospheric Research, Boulder, Colorado, USA, https://doi.org/10.5065/1dfh-6p97, no. NCAR/TN-556+STR, 2021.

Sørensen, J. N. and Myken, A.: Unsteady actuator disc model for horizontal axis wind turbines, Journal of Wind Engineering and Industrial Aerodynamics, 39, 139–149, 1992.

Sorensen, J. N. and Shen, W. Z.: Numerical modeling of wind turbine wakes, J. Fluids Eng., 124, 393–399, 2002.

https://doi.org/10.5194/wes-2025-220
Preprint. Discussion started: 14 November 2025

Tian, L., Song, Y., Xiao, P., Zhao, N., Shen, W., and Zhu, C.: A new three-dimensional analytical model for wind turbine wake turbulence intensity predictions, Renewable Energy, 189, 762–776, https://doi.org/10.1016/j.renene.2022.02.115, 2022.

Vanderwende, B. J., Kosović, B., Lundquist, J. K., and Mirocha, J. D.: Simulating effects of a wind-turbine array using LES and RANS, Journal of Advances in Modeling Earth Systems, 8, 1376–1390, https://doi.org/10.1002/2016MS000652, 2016.

Vollmer, L., Sengers, B. A. M., and Dörenkämper, M.: Brief communication: A simple axial induction modification to the Weather Research and Forecasting Fitch wind farm parameterization, Wind Energy Science, 9, 1689–1693, https://doi.org/10.5194/wes-9-1689-2024, 2024.

Voutsinas, S., Rados, K., and Zervos, A.: On the Analysis of Wake Effects in Wind Parks, Wind Engineering, 14, 204–219, http://www.jstor.org/stable/43749429, 1990.

Wu, S., Archer, C. L., and Mirocha, J.: New insights on wind turbine wakes from large-eddy simulation: Wake contraction, dual nature, and temperature effects, Wind Energy, 27, 1130–1151, https://doi.org/10.1002/we.2827, 2023.

Xie, S. and Archer, C.: Self-similarity and turbulence characteristics of wind turbine wakes via large-eddy simulation, Wind Energy, 18, 1815–1838, https://doi.org/10.1002/we.1792, 2015.

Xie, S. and Archer, C. L.: A numerical study of wind-turbine wakes for three atmospheric stability conditions, Boundary-Layer Meteorol, 165, 87–112, https://doi.org/10.1007/s10546-017-0259-9, 2017.

Zhang, R., Xin, Z., Huang, G., Yan, B., Zhou, X., and Deng, X.: Characteristics and modelling of wake for aligned multiple turbines based on numerical simulation, Journal of Wind Engineering and Industrial Aerodynamics, 228, 105 097, 2022.

Zhu, X., Xiao, S., Narasimhan, G., Martinez-Tossas, L. A., Schnaubelt, M., Lemson, G., Yao, H., Szalay, A. S., Gayme, D., and Meneveau, C.: JHTDB-wind: A web-accessible large-eddy simulation database of a wind farm with virtual sensor querying, Wind Energy Science Discussions, 2025, 1–28, https://doi.org/10.5194/wes-2025-124, 2025.